Investigating Axonal Collateral Branching Through Light Induced Receptor Tyrosine Kinases

A Thesis

submitted to

Indian Institute of Science Education and Research Pune in partial fulfilment of the requirements for the BS-MS Dual Degree Programme

by

Asutosh Routa

Indian Institute of Science Education and Research Pune

Dr. Homi Bhabha Road,

Pashan, Pune 411008, INDIA.

Date: 27th March, 2025

Under the guidance of

Dr Aurnab Ghose

Professor, Biology

From May 2024 to March 2025

INDIAN INSTITUTE OF SCIENCE EDUCATION AND RESEARCH PUNE

Certificate

This is to certify that this dissertation entitled ‘Investigating axonal collateral branching through light induced receptor tyrosine kinases’ towards the partial fulfilment of the BS-MS dual degree programme at the Indian Institute of Science Education and Research, Pune represents study/work carried out by Asutosh Routa at Indian Institute of Science Education and Research under the supervision of Dr Aurnab Ghose, Professor, Department of Biology, during the academic year 2024-2025.

Dr Aurnab Ghose
Date: 27-03-2025

Dr Nagaraj Balasubramanian
Date: 27-03-2025

Committee:
Dr Aurnab Ghose
Dr Nagaraj Balasubramanian

Dedicated to

My Friends and Family

Declaration

I hereby declare that the matter embodied in the report entitled '**Investigating axonal collateral branching through light induced receptor tyrosine kinases**' are the results of the work carried out by me at the Department of Biology, Indian Institute of Science Education and Research, Pune, under the supervision of Dr Aurnab Ghose and the same has not been submitted elsewhere for any other degree. Wherever others contribute, every effort is made to indicate this clearly, with due reference to the literature and acknowledgement of collaborative research and discussions.

Asutosh Routa

20201080

Table of Contents

List of Figures

Abstract

The human brain is formed through billions of neurons establishing precise connections. Collateral branches are fine perpendicular axonal projections, and are crucial for synaptic

connectivity and emerge in response to injury or plasticity. Neurotrophic factors like NGF (high-affinity binding to TrkA) and BDNF (high-affinity binding to TrkB) are known to induce branch formation, yet the spatiotemporal mechanisms remain unclear. Optogenetic Trk variants provide a precise tool to study receptor-mediated changes.

This thesis utilizes Opto-TrkA and Opto-TrkB in chick spinal and DRG neurons to investigate branch formation. Optimizing light intensity revealed an intensity-dependent increase in protrusions. Prolonged stimulation significantly enhanced protrusion density. Additionally, localized Opto-TrkA stimulation was applied for spatiotemporal control of branching.

Eps8, an actin-capping protein, is a key regulator of branch formation. Its knockdown is known to increase protrusions. Here, I examined its role in stabilizing branches and found an increase in stable branches.

Overall, this thesis establishes an optogenetic framework to study collateral branch formation through the precise activation of TrkA and TrkB receptors.

Acknowledgements

I would like to express my sincere gratitude to Dr. Aurnab Ghose for allowing me to undertake this project and for providing access to all the resources. His guidance and insightful discussions have been key in shaping the direction of my research. Despite his busy schedule, he has always made time to offer thoughtful advice, which has been crucial in troubleshooting both technical and conceptual challenges.

I would like to express my sincere gratitude to the microscopy facility, where the majority of my work was conducted. Additionally, I am grateful to Vijay for his support and assistance in overcoming various technical challenges throughout the project.

I am profoundly thankful to every member of the AG Lab, for their invaluable support during discussions and troubleshooting sessions. A special thanks to Shinjini, whose enthusiasm and unwavering support have been a constant source of encouragement, and to Saunri, who was always ready to listen when things didn't go as planned. I would also like to acknowledge Avik, Nikita, Suneha, Roopshali, Indrajit, Usashi, and Shivani for being supportive from the very first day.

I wholeheartedly thank my friends, especially Digvijay, who has been more like an elder brother to me, and Satyabrata, without whom this journey would have been far more challenging. Additionally, I would like to thank Lisas for helping me settle into the lab. Sudeepto and Rushik for all the brainstorming sessions and for being cheerful companions throughout.

Lastly, my parents for their constant support throughout this journey. Despite never having had the opportunity to attend college themselves, they ensured that I never lacked any necessities and stood by me in every way possible.

Contributions

Contributor name	Contributor role
AR and AG	Conceptualization Ideas
AR	Methodology
AR	Software
AR	Validation
AR	Formal analysis
AR	Investigation
AG	Resources
AR	Data Curation
AR	Writing - original draft preparation
AR and AG	Writing - review and editing
AR	Visualization
AG	Supervision
AG	Project administration
AG	Funding acquisition

AR- Asutosh Routa

AG- Aurnab Ghose

Chapter 1 Introduction

1.1 Branching in Axons

The brain, as an organ, plays a central role in orchestrating complex physiological and behavioral functions necessary for an organism's survival. These range from sophisticated sensorimotor activities to endocrine homeostasis, made possible by an intricate network of neurons. Humans have around 86 billion neurons, each forming thousands of synaptic connections, with cortical pyramidal neurons establishing up to ten times more connections (Azevedo et al., 2009). Neurons originate from neural progenitor cells, which undergo migration and differentiation into distinct neuronal subtypes (Hatten, 1999). Once differentiated, these neurons extend axons that polarize toward specific targets, including other neurons and peripheral organs, to establish functional synapses (Polleux and Snider, 2010). Axonal growth and guidance are tightly regulated processes, influenced by trophic factors that can either promote or inhibit extension (Gibson et al., 2011). During this phase, axons give rise to secondary and tertiary branches, significantly enhancing network complexity. These branches can emerge through three primary mechanisms: arborization, growth cone bifurcation, and axon collateral branching as shown in Fig. 1.1 (Gibson and Ma, 2011).

Differential growth rates between the lateral and leading edges of a growth cone can result in growth cone splitting, leading to the formation of two axonal branches in Y or T shapes (Wessells and Nuttall, 1978). This phenomenon occurs when the growth cone encounters inhibitory cues that cause it to divide into two halves. Trophic factor cues such as NT-3 and NGF, secreted by target regions, are often associated with this type of splitting and subsequent branching. Dorsal root ganglion (DRG) neurons frequently arborize at their target sites through this mechanism (Manitt et al., 2009).

Axonal collateral branching is a critical mechanism in vertebrate neurodevelopment (Gibson et al., 2011). Therefore, obtaining a mechanistic understanding of axonal collateral branch formation is crucial for deciphering both neurodevelopmental processes and adult neurogenesis. Trophic factors such as Neurotrophin-3 (NT-3),

Brain-Derived Neurotrophic Factor (BDNF), and Nerve Growth Factor (NGF) play key roles in mediating cytoskeletal changes that facilitate axonal collateral branch formation (Lykissas et al.2007). In the following sections, we will explore the role of NGF and BDNF in axonal branching in greater detail.

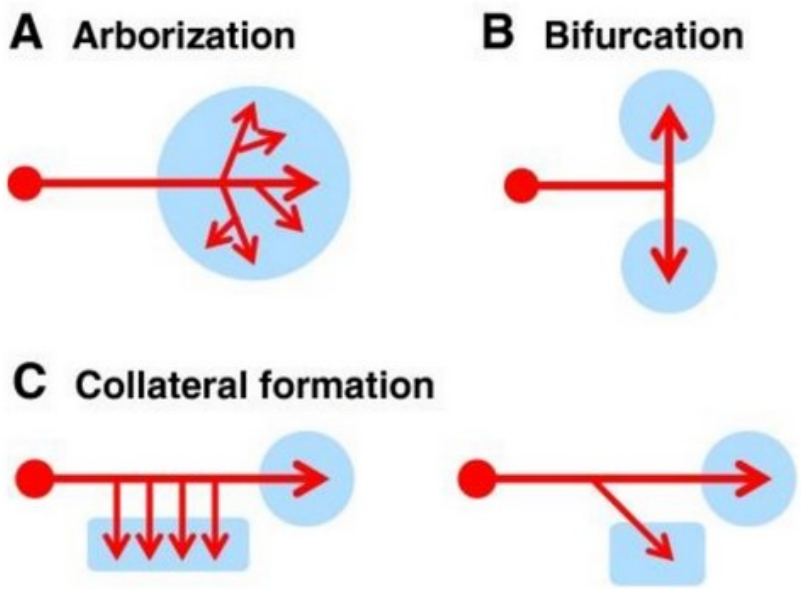

Figure 1.1 Different forms of axonal branching. A) Arborization is used to establish multiple connections at the target site in response to the release of cues like NGF and NT3. B) Bifurcation is the splitting of the growth cone, taking the form of 'Y'- or 'T'-shaped branches. C) Collateral branching is the formation of protrusions through the axon shaft. Figure reproduced from Gibson and Ma (2011).

1.2 Collateral Branching in Axons

The *de novo* emergence of axonal collateral branches during development is crucial for establishing multiple synaptic connections (Gallo, 2011). Axonal collateral branching is a highly dynamic and multimodal process (Armijo-Weingart and Gallo, 2017), which we will explore step by step. The specificity of synaptic and neuromuscular connections plays a fundamental role in maintaining homeostatic control by enabling multiple target innervations to synchronize diverse physiological functions (Li et al., 2024). Due to the intricate molecular and cellular coordination involved, axonal collateral formation is tightly regulated by multiple factors. Disruptions in this regulation can result in excessive branching, leading to pathophysiological consequences (Shafi et al., 2015). For

instance, hyperactivation of the RHEB/mTOR pathway enhances axonal connectivity, which has been linked to epileptic seizures (Proietti Onori et al., 2021).

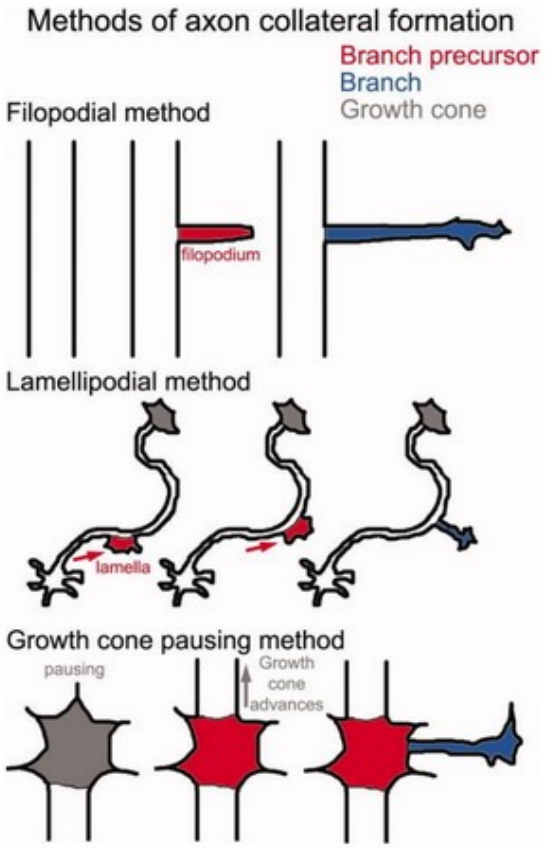

Figure 1.2 Mechanism of axonal collateral branching. A) Filopodial-based collateral branching: formation of a finger-like projection called filopodia on the membrane, which gets stabilized by interaction with microtubules. B) Lamellipodia-based method: forming growth cone-like waves along the axon. C) The stoppage points of the growth cone waves demarcate a branch point. The growth cone pausing mechanism involves the formation of collaterals at spots where growth temporarily stops. Figure reproduced from Gallo (2011).

In adults, collateral branching is often triggered by injury and contributes to plasticity, repair, and regeneration to restore target connections (Liu et al., 2012; Yu et al., 2016). However, the regenerative potential of different neuronal sub-groups varies due to differences in accessory and inhibitory factors within cellular and extracellular matrices (Chelyshev et al., 2022). This remains an active area of research.

There are three known mechanisms of branch formation from axons (Gallo, 2011): filopodial-based, lamellipodial-mediated, and filopodia-based extension. Growth cone pausing at specific points often leads to the formation of filopodia-like structures with high protrusive activity (Szebenyi et al., 1998). Actin-based, thin, sheet-like membrane protrusions known as lamellipodia have been associated with growth cone waves in hippocampal neurons and are known to promote branching (Flynn et al., 2009). However, filopodial-based protrusions are the most common mechanism for collateral branch formation. These thin, finger-like, actin-based projections emerge from the axonal shaft and are subsequently stabilized by interactions with microtubules, leading to their maturation into branches (Fig 1.2).

Both filopodia and lamellipodia are actin-rich cytoskeletal structures that respond to focal induction by trophic factors. Previous studies have shown that NGF stimulation increases the presence of F-actin patches along the axon shaft, which act as precursors to filopodial projections, highlighting NGF's role in regulating axonal filopodia (Gallo and Letourneau, 1998). Similarly, BDNF-coated beads have been reported to induce lamellipodia-like sprouting along the axon shaft, at the site of contact in neuronal cultures (Gallo and Letourneau, 1998). Given this, the following discussion will primarily focus on collateral branch formation through NGF- and BDNF-induced signaling.

1.3 NGF and its Influence in Axonal Collateral Branching

Neuronal Growth Factor (NGF) is a dimeric neurotrophin that plays an integral role in the growth, survival, and differentiation of neurons. It exhibits strong binding affinity to the Tyrosine Kinase Receptor A (TrkA) and is essential during neurodevelopment, promoting neuronal growth, fate determination, dendritic structure formation, and pruning (Huang and Reichardt, 2003). Upon binding to TrkA, NGF induces receptor dimerization, leading to retrograde transport of the NGF-TrkA complex to the soma, where it triggers local and cell-wide effects (Zweifel et al., 2005). This regulation occurs largely in an activity-independent manner (Ulrich et al., 1998). Additionally, NGF plays a role in axonal pathfinding, ensuring precise innervation of synaptic targets.

NGF signaling induces both local and global cellular changes, ultimately converging on cytoskeletal remodeling and effector protein localization, which drive branch formation. NGF-mediated TrkA dimerization leads to phosphorylation and activation of several downstream signaling pathways. These include the MAPK/ERK pathway, which regulates neuronal differentiation and gene expression; the PI3K/Akt pathway, which promotes cell survival and growth; and the PLCγ pathway, which modulates calcium signaling and cytoskeletal rearrangement (Huang and Reichardt, 2003). Additionally, Rho GTPases, such as Rac1 and Cdc42, play a central role in branch formation, a topic that will be discussed extensively in the following sections (Ketschek et al., 2010). Many of these signaling cascades depend on the endosomal transport of NGF-TrkA vesicles (Harrington and Ginty, 2013).

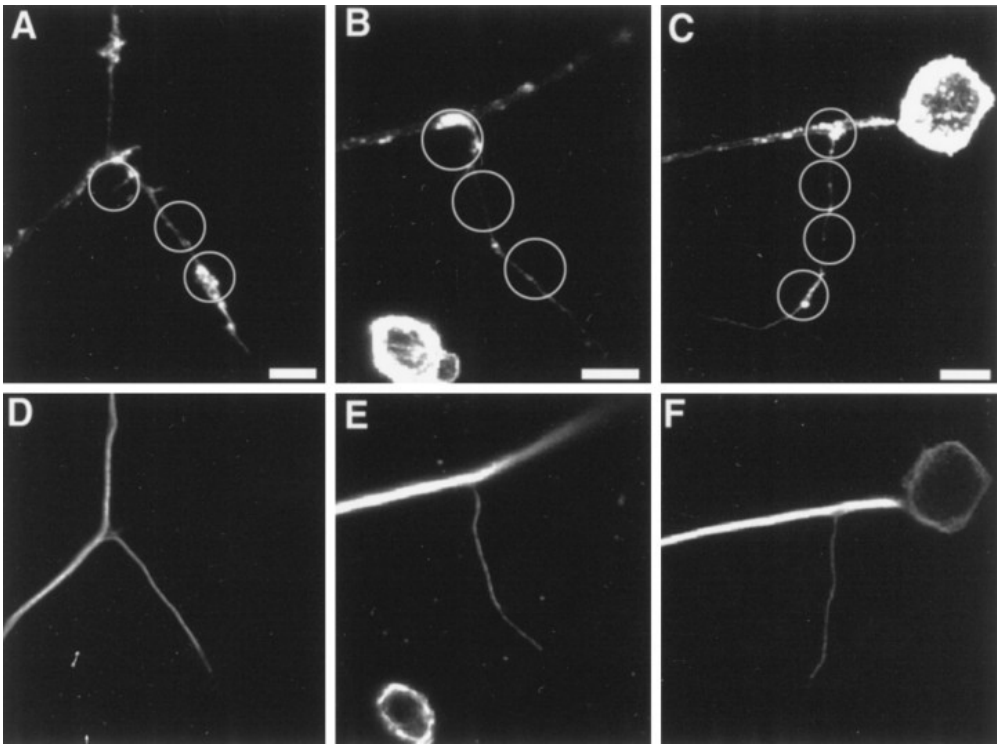

Figure 1.3 Local NGF and BDNF stimulation leads to branch formation. A) Circular representation shows NGF-coated beads. B) Formation of collateral branches at the region of contact of these beads across the axon. C) Panels A–C show rhodamine-phalloidin (conjugated with Alexa 568) staining of F-actin. Scale bar: 10 μm. Figure reproduced from Gallo and Letourneau (1998).

NGF-induced collateral branch formation is crucial for both neurodevelopment and adult neurogenesis. Embryonic chick DRG neurons cultured in an NGF-rich environment exhibit increased collateral branching (Gallo and Letourneau, 1998). Similarly, NGF derived from vascular smooth muscle cells (VSMCs) has been shown to regulate sympathetic collateral branching, facilitating blood vessel innervation in embryonic skin (Li et al., 2024). Conversely, NGF depletion leads to attenuated collateral sprouting of tooth-pulp axons and cutaneous mechanoreceptive axons in ferrets (Doubleday and Robinson, 1994).

NGF-TrkA signaling plays an important role in injury-induced collateral branching, helping to restore lost connections following neuronal damage (Mearow, 1998). Studies have revealed elevated levels of NGF and other trophic factors in lesioned tissue (Zheng and Tuszynski, 2023). As previously discussed, TrkA activation promotes axonal regeneration and collateral branching via downstream signaling intermediates such as Rho GTPases. Additionally, local application of anti-NGF antibodies has been shown to inhibit collateral sprouting in rats induced by prolonged constriction injury of the sciatic nerve (Ro et al., 1996).

Structural changes resulting from chronic NGF-TrkA activation post-injury can also lead to pathological outcomes. Excessive axonal sprouting, synapse remodeling, and collateral branching within pain perception pathways may contribute to neuropathic pain conditions, where aberrant axonal growth and miswiring in the spinal cord result in persistent pain and hypersensitivity (Cotman, 1999). The TrkA-induced cAMP-PKA pathway has also been shown to contribute towards overcoming inhibitory signals in injured environments (Atkins et al., 2007).

1.4 BDNF in Axonal Collateral Branching

BDNF (Brain-Derived Neurotrophic Factor), which primarily binds to Tyrosine Kinase B (TrkB) receptors, is a neurotrophin similar to NGF and plays a central role in axonal pathfinding and collateral branching in sensory and cortical neurons during neurodevelopment (Cohen-Cory et al., 2010). Unlike NGF, which is secreted by target cells, BDNF is released by surrounding cells in an activity-dependent manner. This

allows BDNF to regulate synapse formation and strengthening in real-time, fine-tuning neuronal connectivity alongside NGF (Miyasaka and Yamamoto, 2021).

BDNF-coated beads were found to induce actin-based structures at sites of contact with the axonal shaft in chick DRG cultures (Gallo and Letourneau, 1998). BDNF has also been implicated in axonal regeneration and remodeling. Intraocular application of BDNF was observed to enhance ectopic branching and stimulate collateralization in regenerating optic fibers (Dawson et al., 2015). Further, BDNF exhibits a differential modulatory role in neuronal morphology. *In vivo* studies on retinal ganglion cells (RGCs) show that BDNF contributes to reduced dendritic arborization while increasing axonal arborization (Lom and Cohen-Cory, 1999).

Similar to NGF induction, Rho GTPases like Rac1 and Cdc42 induce cytoskeletal remodeling by promoting actin patch formation. Additionally, BDNF-TrkB signaling also activates RhoA, which is crucial for dendritic spine remodeling and synaptic stability (Hedrick et al., 2016).

1.5 Cytoskeletal Regulation in Axonal Collateral Branching

Cytoskeletal remodeling is a fundamental mechanism driving axonal collateral branching (Gallo, 2011). Branch formation is a stepwise process involving patch formation, patch stabilization, and filopodial protrusion (Kalil and Dent, 2014). The neurotrophins NGF and BDNF mediate this process through TrkA and TrkB receptor activation, respectively, triggering downstream signaling cascades that converge on Rac1 and Cdc42—key regulators of cytoskeletal remodeling. Localized activation of Rac1 and Cdc42 promotes actin polymerization at focal points along the axon, leading to the formation of actin-based hotspots or actin patches. These patches provide the structural foundation for the emergence of protrusive branching precursors.

Rac1 activation facilitates actin filament polymerization via actin-binding effector proteins such as Arp2/3, Formin-2 (Fmn2), and Ena/VASP (Gallo, 2011). While Arp2/3 mediates the branching of actin filaments, Fmn2 nucleates and elongates them. The interplay between these proteins is both competitive and cooperative, contributing to patch stabilization and filopodial elongation. Capping proteins like Eps8 negatively

regulate filament elongation by binding to actin barbed ends, preventing Fmn2-mediated extension and thereby limiting patch polymerization (Gallo, 2011). Additionally, cofilin modulates actin turnover through depolymerization, underscoring the dynamic and transient nature of actin patches during branch formation.

Microtubule severing proteins such as katanin and spastin are locally recruited to branch formation sites, where they regulate microtubule dynamics. Katanin, guided by signaling cues, facilitates microtubule entry into emerging branches by severing microtubules at branch points, enhancing polymerization. Spastin, in contrast, promotes disassembly and reorganization of microtubule fragments, ensuring cytoskeletal adaptability (Yu et al., 2008). The interplay between actin remodeling and microtubule severing establishes a dynamic framework essential for stabilizing and extending axonal collateral branches.

Despite these insights, the precise temporal coordination of these molecular players in live axonal branching remains poorly understood.

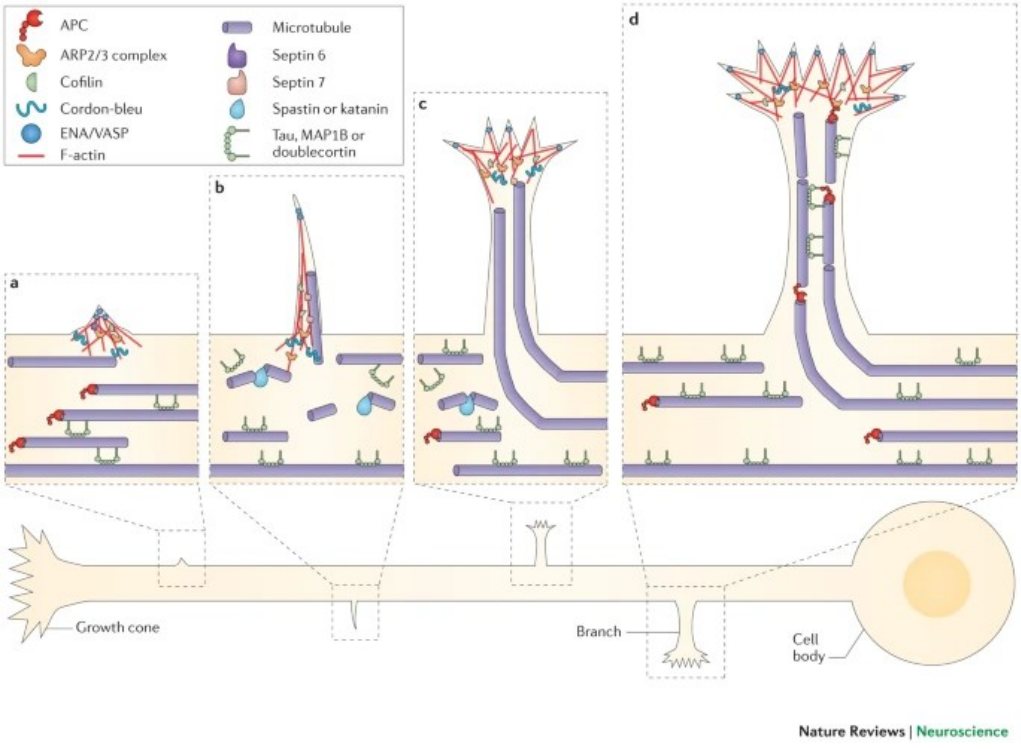

Figure 1.4 Stages of branch formation. A) Patch formation. B) Early immature protrusion. C) Branch stabilization through microtubule invasion. D) Further stabilization and maturation. Figure reproduced from Kalil and Dent (2014).

1.6 Optogenetic Trk receptors

While extensive research has established the roles of NGF-TrkA and BDNF-TrkB in axonal collateral branching, a critical gap remains in our understanding of how these signaling events are coordinated in a spatiotemporal manner. Given this is a ligand mediated local induction, the localized recruitment and activation of downstream effectors at specific axonal sites suggest a finely tuned regulatory mechanism, but the dynamic interplay of these factors remains elusive due to the limitations of conventional biochemical and genetic approaches.

Optogenetic stimulation has recently been employed to study receptor-mediated signaling pathways due to its significant advantages over traditional ligand-based approaches. One of its key benefits is the ability to achieve unparalleled spatiotemporal resolution, with some systems offering millisecond-scale control over receptor activation. In contrast, ligand-based methods are constrained by diffusion and clearance times, limiting their precision in studying transient signaling events. Furthermore, many cellular processes require localized receptor activation at specific subcellular compartments, which remains challenging with traditional approaches (Karunarathne et al., 2015). Optogenetic tools overcome this limitation by enabling targeted spatial control of receptor activation (Kramer et al., 2021). Another advantage is the ability to reversibly and repeatedly stimulate receptors using light pulses, unlike ligands, which require washing out or enzymatic degradation for deactivation (Cokić et al., 2021). Additionally, optogenetic stimulation allows fine-tuned modulation of receptor activity by adjusting light intensity and duration, whereas ligand-based methods often lead to receptor saturation, making graded control difficult. Finally, optogenetics is highly compatible with fluorescence imaging for real-time monitoring of cellular responses, whereas traditional ligands can introduce autofluorescence or require labeling, which may interfere with imaging.

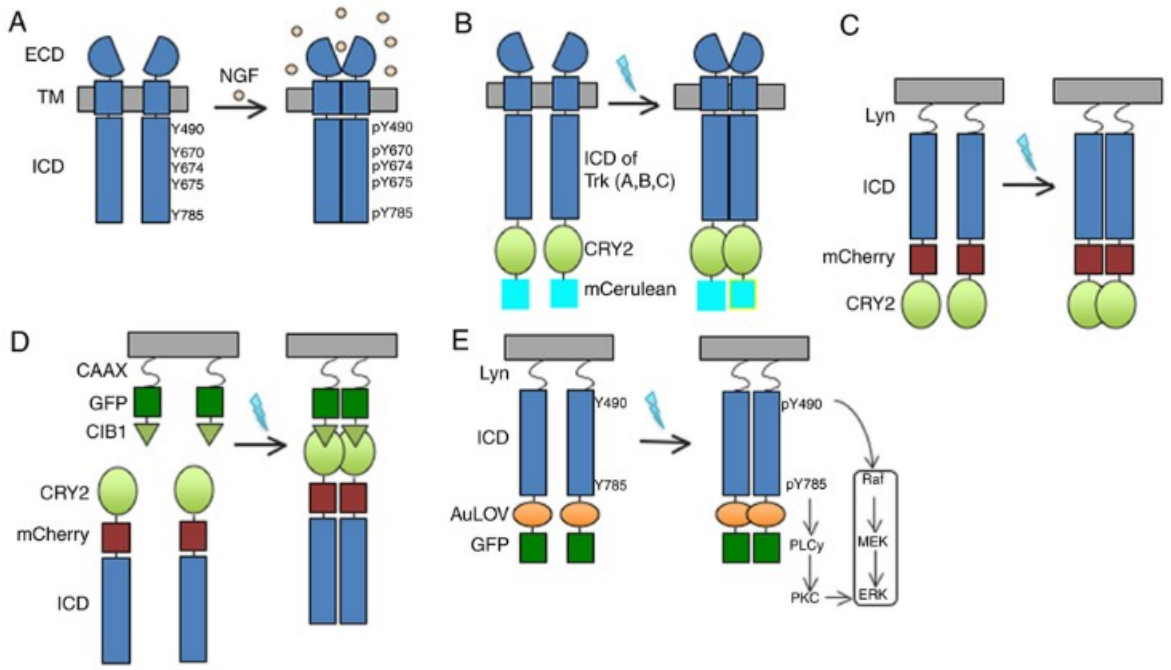

Figure 1.5 Different forms of optogenetic constructs of Trk receptors. A) Wild-type. B) C-terminal fused with the CRY2 photoactivatable dimerizing domain. C) Extracellular and intermembrane domains removed and replaced with a lipidation Lyn moiety. D) CIB1-GFP-CAAX replaces the Lyn sequence for membrane targeting. E) Similar to C, but the AuLoV domain is used for light-induced dimerization. Schematic sourced from Wei Zhang et al. (2022).

Trk receptors exist as monomers but dimerize upon binding extracellular ligands, triggering phosphorylation of key tyrosine residues and activating downstream signaling pathways. Given their physiological significance, Trk receptors have been engineered to be light-sensitive, allowing for a more controlled investigation of their function. This is achieved by incorporating photosensitive dimerizing domains that facilitate receptor clustering upon light exposure. For instance, the Photolyase Homology Region (PHR)—a light-sensitive domain derived from cryptochrome proteins such as CRY2 from *Arabidopsis thaliana*—mediates blue light-dependent dimerization and clustering, thereby activating signaling pathways (Fig. 1.5B). To overcome certain challenges, these engineered receptors have undergone several modifications over time. For example, the transmembrane and extracellular domains have been removed and replaced with a lipidation Lyn moiety to prevent endogenous ligand-induced activation (Fig. 1.5C). Additionally, substituting the Lyn moiety with CIB1-GFP-CAAX enables even

more localized receptor dimerization (Fig. 1.5D). Each of these modifications presents distinct advantages and limitations (Wei Zhang et al., 2022).

Given the spatiotemporal specificity of Trk receptor activation, which is crucial for physiological function, recent studies have increasingly employed light-inducible Trk receptor variants to investigate receptor activation-mediated phenomena. A study demonstrated that specific tyrosine residues (Y490 and Y785) on TrkA contribute additively to cell differentiation through the ERK pathway (Khamo et al., 2019). This approach allowed for the precise dissection of TrkA signaling subcircuits without interference from other receptors. By fusing the intracellular domain of TrkA (iTrkA) to the photoreceptor CRY2, a study showed the characterization of the downstream signaling cascades, such as the Raf/MEK/ERK and PI3K/Akt pathways, in NIH 3T3 cells (Duan et al., 2018). Furthermore, one group also attempted localized activation of TrkB receptors using a light-inducible TrkB variant to study actin blobs during neurite formation (Nithianandam and Chien, 2018).

Thus, optogenetic variants of TrkA and TrkB serve as valuable tools for investigating axonal collateral branching, as their responses closely align with ligand-mediated experiments reported in multiple previous studies.

1.7 Objectives

In this thesis, Opto-TrkA and Opto-TrkB will be utilized to examine the mechanisms underlying collateral branch formation.

1. Standardize light intensity for optimal stimulation of optogenetic tyrosine kinase receptors (Opto-TrkA and Opto-TrkB).
2. Investigate the ability of Opto-TrkA and Opto-TrkB to induce axonal collateral branching in chick spinal and DRG neurons.
3. Examine local activation of chick spinal neurons to promote branch formation.
4. Determine the effect of Eps8 knockdown on mature branch formation in chick spinal neurons.

Chapter 2 Materials and methods

2.1 Materials

The materials utilized in this study include: 22 mm circular coverslips, 35 mm culture plates, and silicone sealant (Dow Corning) for culture preparation. Coating reagents included Poly-D-lysine (10 mg/ml; PLL). Cell culture media and supplements consisted of 1x Trypsin-EDTA solution, L-15 medium, 10X PBS, 100x Penicillin-Streptomycin (Penstrep), Hi-FBS (Fetal Bovine Serum), Methocel powder, and 1x Opti-MEM. Fixatives and staining reagents included 4% paraformaldehyde (PFA), 1N HCl, and Triton-X-100. Immunostaining was performed using a Beta-3 tubulin antibody, Alexa Fluor 647 goat anti-rabbit secondary antibody, and Alexa Fluor 568 phalloidin. Additional consumables included albumin from bovine serum (lyophilized powder), a 0.2 µm syringe filter, and a 50 ml syringe.

2.2 Primary neuron culturing

6 day old chick spinal cord tissues were dissected out in 1xPBS . Trypsinization of the obtained tissues was followed after this (0.05% Trypsin-EDTA (Lonza, HiMedia) at 37C for a span of 15 to 20 minutes. This is re-suspended again in Optimem(Gibco) before cuvette-mediated electroporation (CUY21SC,Nepagene); respective amount of plasmid was also added. After successful transfection, the neurons were cultured on 35 mm plastic dishes with glass bottoms, followed by an incubation at 37C for 24-36 hours in L-15 medium with 5% fetal bovine serum (GBS;Gibco) and 1x penstrep (Gibco). The dishes are coated with PDL(Poly-D-Lysine). For chick dorsal root ganglion(DRG) tissue culture, 8 day old embryos were used. Further rest of the methodology remains similar as for chick spinal culture.

2.3 Transfection with plasmids

The following plasmids were used in this study: pCAG-Opto-TrkA-mCitrine (Chang et al., 2014), cloned into the pCAG vector by Lisas Sewatkar; pCAG-F-tractin-mCherry

(Addgene #58473); and pCAG-GFP (Addgene #11150). Additionally, Lyn-cytTrkB-PHR-mCitrine (Opto-cytTrkB) and Opto-cytTrkB (Y515F) (Woo et al., 2019) were cloned into the pCAG vector by me. All plasmids were obtained using alkaline lysis.

2.4 Electroporation

Transfections were performed using the NEPA21 Type II square-wave electroporator. Two types of electrical pulses were applied to the cuvette: Poring Pulse – A high-voltage, short-duration pulse (150V, 5 ms pulse length, 50 ms pulse interval, 10% decay rate) was applied to induce pore formation in the cell membrane, facilitating the entry of nucleic acids. Transfer Pulse – A low-voltage, alternating-polarity pulse (20V, 50 ms pulse length, 50 ms pulse interval, 40% decay rate) was subsequently applied to promote the movement of charged particles (DNA or morpholinos), increasing the likelihood of successful transfection. The amount of plasmid DNA used for transfection was optimized based on plasmid size and fluorescence intensity post-transfection. Morpholinos were transfected at a standard concentration of 100 μM.

Eps8 splice blocking morpholino - CAAGGGGACTGTGAGTTGTGCTGCA
Standard control morpholino - CCTCTTACCTCAGTTACAATTTATA

2.5 RT-PCR

RNA isolation from primary spinal neuron cultures was performed using a column purification method, which relies on the binding of nucleic acids to a silica matrix under high salt conditions and their subsequent elution under low salt conditions. The protocol began with the isolation of the tissue of interest, subsequently, 350 μL of lysis buffer was added, followed by thorough homogenization. The lysate was subjected to centrifugation at 13,000 rpm for 3 minutes, after which the supernatant was collected and mixed with 350 μL of 70% ethanol. The mixture was then centrifuged at 10,500 rpm for 30 seconds, after which the flow-through was discarded, and 700 μL of RW1 buffer was added. Following another centrifugation at 10,500 rpm for 30 seconds, the flow-through was discarded, and two sequential washes with 500 μL of RPE buffer were

performed, with the second wash including a 2-minute centrifugation to remove residual salts. A blank spin was conducted for 2 minutes at 10,500 rpm before eluting the RNA with 20 µL of RNase-free water. The isolated RNA was then converted to cDNA using the Takara PrimeScript cDNA synthesis kit, which included 2 µL of 5X PrimeScript buffer, 0.5 µL of Oligo dT primer, 0.5 µL of Random 6 Hexamer, and 6.5 µL of RNA, making a total reaction volume of 10 µL. This mixture underwent a thermocycling process to synthesize cDNA. For polymerase chain reaction (PCR), A 10 µL reaction mixture was prepared, including 1 µL of 10X Taq buffer, 0.8 µL of dNTPs, 0.2 µL each of forward and reverse primers, 0.2 µL of Taq polymerase enzyme, 1.5 µL of cDNA, and 6.1 µL of nuclease-free water. PCR was performed using a standardized Taq cycle in a thermocycler. To determine the optimum annealing temperature for plasmid amplification, a gradient PCR was conducted, and 57.5°C was identified as the optimal temperature.

Forward Primer (5' - GCAATCAGTGACAGCAAGAG - 3')

Reverse Primer (5' - TGACCATGAGGAAACGGC - 3')

2.6 Immunocytochemistry

Cells fixed with 4% PFA, followed by 3 washes in 1XPBS at a 10 min interval. Cells permeabilized with 0.1% Triton(in 1XPBS) for 10 minutes followed by 3 washes at an interval of 5 minutes. Blocking was done with 3% (W/V in 1XPBS) BSA was used. Further incubation with primary antibody of β3-tubulin for 12 hours in 4°C overnight. Followed by 3 wishes in 1XPBS and then incubated with a secondary antibody (ALexa 647) and Alexa phalloidin 568 (1:100) for 2 hours, followed by 3 washes using 1XPBS. For the sets where only phalloidin staining ws needed, Alexa phalloidin 568 (1:100) was incubated after blocking, and then washed after 2 hours with 1XPBS.

2.7 Imaging

The photomicrographs were acquired using Leica SP8 confocal system with 60x,oil objective. Ziess Multiphoton with 60x oil immersion objective was used for live imaging experiments for local activation. The temperature was maintained at 37 oC using.

2.8 Global activation setup

Chick spinal neurons were transfected with pCAG-Opto-TrkA-Citrine and pCAG-Opto-TrkB-mCitrine. For globally activating all neurons that have the construct, the culture dish was placed inside a custom-made Blue light LED lightbox. An Arduino controlled the blue light LEDs operated via an in-house code. Eight 5mm blue lights (470nm, 100mW power dissipation) were arranged on a breadboard. Culture dishes were placed 2.5cm from the LEDs. Each culture dish had 2 LEDs above them. The pattern for globally activating neurons was 2 seconds ON and 5 seconds OFF. This pattern was repeated for 35, when cultures after plating incubated for 1 hour at 37°C, were transferred to the light induction setup. There was a 12hr gap between the start of the pattern and the time the culture dish was incubated within the box so that enough time was given for the construct to give expression.

2.9 Local activation setup

Local activation of spinal neurons transfected with Opto-TrkA-Citrine and F-tractin-mCherry was done on Zeiss multiphoton confocal system using a 488 laser. The neuronal culture was placed inside a stage incubator set at 37 oC. Firstly a transfected neuron was located, having minimal to no protrusive activity, then acquired for 10 minutes(one snap every 10 seconds) and then Square ROIs were marked (on the region of least protrusive activity) on individual neurons, and they were activated using laser power of 200 µW/cm² and the ROI was assigned for the stimulation program. The stimulation pattern was 500 millisecond activation using a 488 laser every 9 seconds for 30mins.

2.10 Image analysis

All image analyses were conducted using FIJI ImageJ software. Morphometric assessments were performed manually by scoring with the segmented freehand tool in FIJI ImageJ. Integrated density, which represents the sum of pixel intensity values within a selected region, is equivalent to the product of the area and the mean gray

value. This parameter was utilized to quantify F-tractin accumulation within the region of interest (ROI) corresponding to activation.

2.11 Statistical analysis

All graphical representations and statistical analyses were carried out using GraphPad Prism 8. Data visualization was performed using violin plots, where the central line represents the mean, and error bars denote the standard error of the mean (SEM). Comparisons between two groups were conducted using the Mann-Whitney test.

Chapter 3 Results

3.1.1 Optogenetic activation of Opto-TrkA and Opto-TrkB

NGF-TrkA and BDNF-TrkB signaling has been studied for having various developmental roles, from growth and morphogenesis to cell survival. Growing neurons in NGF-stimulated environment was shown to promote protrusion formation through PI3K based localised microdomains (Andrea Ketschek et al., 2010). Further, NGF has also been associated for focal debundling of microtubules for invasion into nascent protrusions (Ketschek et al., 2015). Similarly, growing neurons in a BDNF stimulated environment over short term promotes axon shaft elongation but little to no branching (Kellner et al., 2014). While long term BDNF exposure was seen to result in increased axonal collateral branching and arborization (S and Se, 1995; Granseth et al., 2013). Further, as previously discussed, they result in local cytoskeletal remodeling to promote axonal collateral branches in chick sensory neurons (Gallo and Letourneau, 1998). But NGF and BDNF are prone to degradation in *in-vitro* culture environments. Secondly both of the neurotrophins are known to bind to more than one receptor (although might vary in affinity), but such kind of combinatorial activation is responsible for multitude of signalling factors which vary in their physiological responsiveness (Huang and Reichardt, 2003). Furthermore, NGF and BDNF are prone to diffusion, leading to widespread receptor activation. This poses a challenge in studying the transient downstream processes resulting from localized receptor activation for collateral branching. Use of optogenetic variants (section-1.6) of TrkA and TrkB can potentially address this issue due to their precise spatiotemporal control. Optogenetic activation is specific to a single receptor type, which enables a controlled and precise analysis of receptor induction and its corresponding downstream effects.

Considering the above discussion, optogenetic activation of TrkA and TrkB serves as a powerful tool to study collateral branch induction, given its spatiotemporal specificity in receptor-induced signaling cascades. In this thesis, Opto-TrkA and Opto-TrkB will be utilized to examine the mechanisms underlying collateral branch formation. Opto-TrkA consists of a PHR-CRY2 unit, which undergoes light-induced dimerization as described

earlier, whereas Opto-TrkB features a Lyn moiety replacing the extracellular and transmembrane domains. Both variants have been shown to activate key signaling cascades, including PI3K and MAPK/ERK, upon light stimulation (Chang et al., 2014, Woo et al., 2019) (Fig. 3.1).

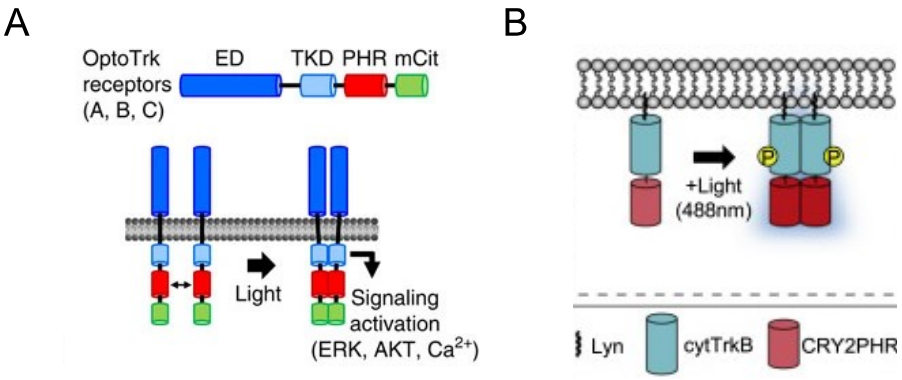

Figure 3.1 Schematic of Opto-TrkA A) and Opto-TrkB B). The CRY2PHR domain facilitates dimerization in both. While Opto-TrkA consists of the full-length Trk receptor, Opto-TrkB comprises only the intracellular domain fused with Lyn and CRY2PHR. Figure reproduced from Chang et al. (2014) and Woo et al. (2019).

3.1.2 Standardization of Light Intensity for Controlled Optogenetic Activation and Survivability

To validate the phenotypic effects of light stimulation in neurons transfected with optogenetic constructs, I first standardized the light power used for stimulation. Heat induced from constitutive stimulation of LED (Light Emitting Diodes) lights can act toxic to neurons, hence influencing cellular viability. Thus, it is fundamental to determine and standardize an optimal power level that ensures efficient stimulation while minimizing any potential cytotoxic effects. To evaluate the heat-induced toxicity of light exposure, a quantitative assessment was conducted. Specifically, the ratio of neuronal cells with neurites to those without neurites was quantified within a single field of view in chick spinal neurons transfected with Opto-TrkA and fixed at the 16-hour time point (Fig. 3.1). Neuronal cell bodies extend fresh neurites upon primary culturing and incubation, facilitating their growth and development. However, heat induced cytotoxicity affects the formation of these neurites.

Primary chick embryonic spinal neurons transfected with Opto-TrkA were plated on poly-D-lysine (PDL)-coated dishes and incubated at 37°C for one hour. Following incubation, the culture dishes were transferred to an Arduino-controlled global light stimulation setup maintained at 37°C. This setup, designed and developed by Lisas Sewatkar, consisted of blue LED lights operating on a on/off cycle of 2s/3s. The neurons were subjected to this stimulation for 16 hours (Fig. 3.2).

After 16 hours of stimulation, the cultures were fixed and imaged. Micrographs were acquired at a 20X objective, capturing a wider field of view encompassing approximately 70–80 cells per image. Among the observed neurons, some exhibited neurite outgrowth, while others did not. The ratio of neurons with neurites to those without neurites was quantified. This measurement was compared across cultures grown at four different light stimulation intensities (400, 300, 180, and 100) varied by adjusting the distance of the light source from culture plates, and later measured using a power meter (Fig. 3.2).

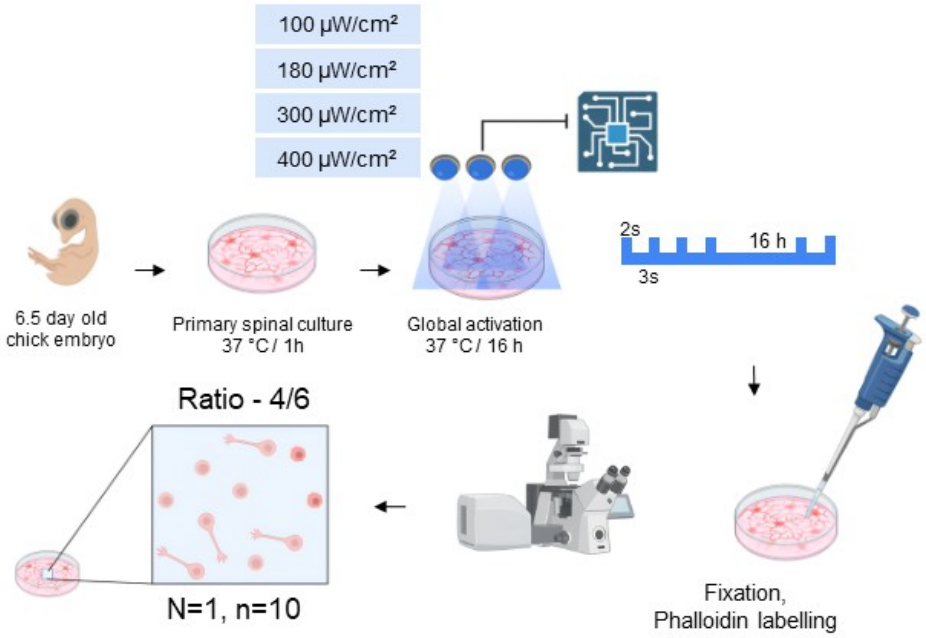

Figure 3.2 Schematic of protocol for global activation with varying light intensities for survivability assessment in chick spinal neurons transfected with Opto-TrkA and the analysis (which included counting the number of cells with neurites to the number of cells without) after 16 hours of stimulation. N represents a single field of view (20× objective), while n denotes the total number of cells analyzed. Created in https://BioRender.com

Neuronal cells subjected to the highest light intensity (400 μW/cm²) exhibited the poorest health, with a significant reduction in neurite outgrowth. This was quantitatively represented by a neurite-bearing to neurite-deprived cell ratio of 0.2, indicating that the majority of cells failed to extend neurites. With the decrease in light intensity, a progressive improvement in neurite outgrowth was observed. At 180 μW/cm², the ratio increased to approximately 0.6, suggesting an enhanced propensity for neurite extension. Notably, at the lowest intensity tested (100 μW/cm²), the number of neurite-bearing cells was comparable to or exceeded the number of neurite-deprived cells, reflecting improved cell viability and neurite outgrowth under these conditions (Fig. 3.3).

With this observation, 180 μW/cm² and 100 μW/cm² were further tested under Arduino-controlled global activation setup, to test if the optogenetic Trk receptors yield any intensity dependent phenotypic effect.

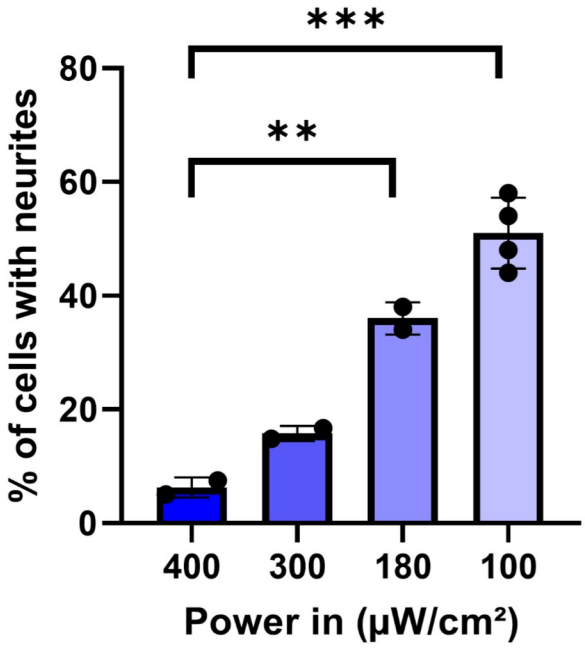

Figure 3.3 A significant difference in the percentage of cells with neurites observed at 100 μW/cm² as compared to 400 μW/cm² denoting improved survivability, no significance was observed in between the other light intensities. A Mann-Whitney U test was conducted, with n = 84 for 400 μW/cm², n = 70 for 300 μW/cm², n = 75 for 180 μW/cm², and n = 124 for 100 μW/cm². $p < 0.01$. N represents a single field of view (20× objective), while n denotes the total number of cells analyzed.

3.1.3 Light intensity dependent increase in protrusion density in chick spinal neurons transfected with Opto-TrkA

Optogenetic proteins are usually seen to exhibit an intensity-dependent response to light stimulation. To analyze the effect of varying light intensity on neuronal morphology, primary chick embryonic spinal neurons were electroporated with Opto-TrkA and plated on poly-D-lysine (PDL)-coated dishes. The cultures were incubated at 37°C for one hour before being transferred to an Arduino-controlled global activation setup, maintained at 37°C. Neurons were subjected to light stimulation (two light intensities: 180 μW/cm² and 100 μW/cm²) for 35 hours, starting one hour after plating, further fixed with 4% paraformaldehyde (PFA) (Fig. 3.4).

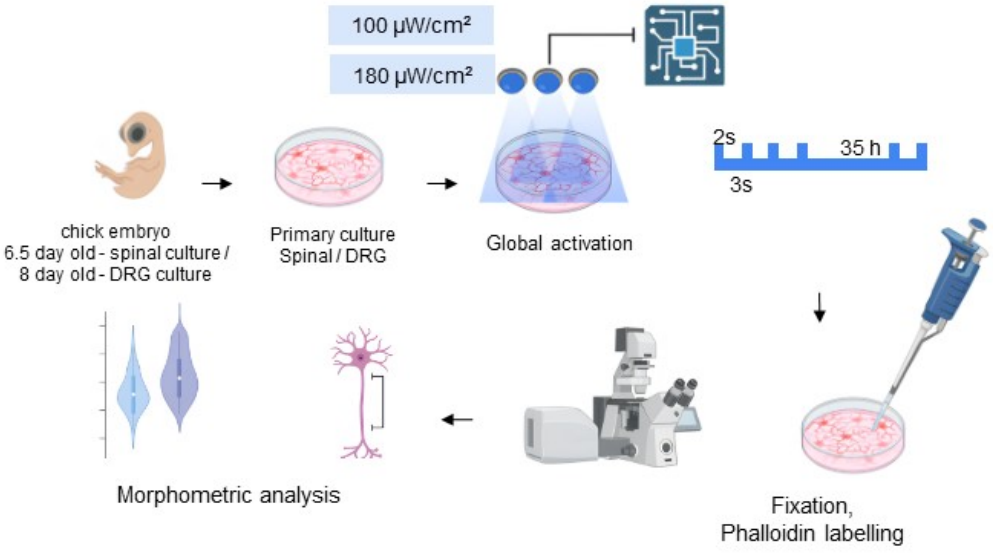

Figure 3.4 Schematic of the protocol for global activation setup in chick spinal/DRG neurons transfected with Opto-TrkA/Opto-TrkB/Opto-TrkB-Y515F/GFP. Created in https://BioRender.com

For cytoskeletal visualization, neurons were stained with Alexa Fluor 568-conjugated phalloidin, which labels F-actin. Given ~20% transfection efficiency of electroporation, only cells expressing Opto-TrkA-mCitrine were analyzed. Morphometric parameters, including protrusion density (number of neurons pre axon shaft/corresponding length of

the axon) were quantified. This analysis was conducted for two light intensities: 180 µW/cm² and 100 µW/cm², and the results were compared. For the control condition, neurons in the culture were processed identically, except that they were incubated (37°C) in dark for 36 hours total.

Light stimulation of Opto-TrkA-transfected neurons resulted in a higher number of protrusions per unit axon length (total number of protrusions/total axonal length of the neuron). Notably, increasing light intensity led to an increase in protrusion density (Fig. 3.5). Among the tested intensities, 180 µW/cm² yielded a higher protrusion density compared to 100 µW. Based on these two observations (Fig. 3.5 and 3.4), while 100 µW/cm² provided better neuronal survival and tolerance, Opto-TrkA stimulation at 180 µW/cm² was more effective in inducing protrusions. Therefore, 180 µW/cm² blue light was used for subsequent optogenetic stimulation experiments.

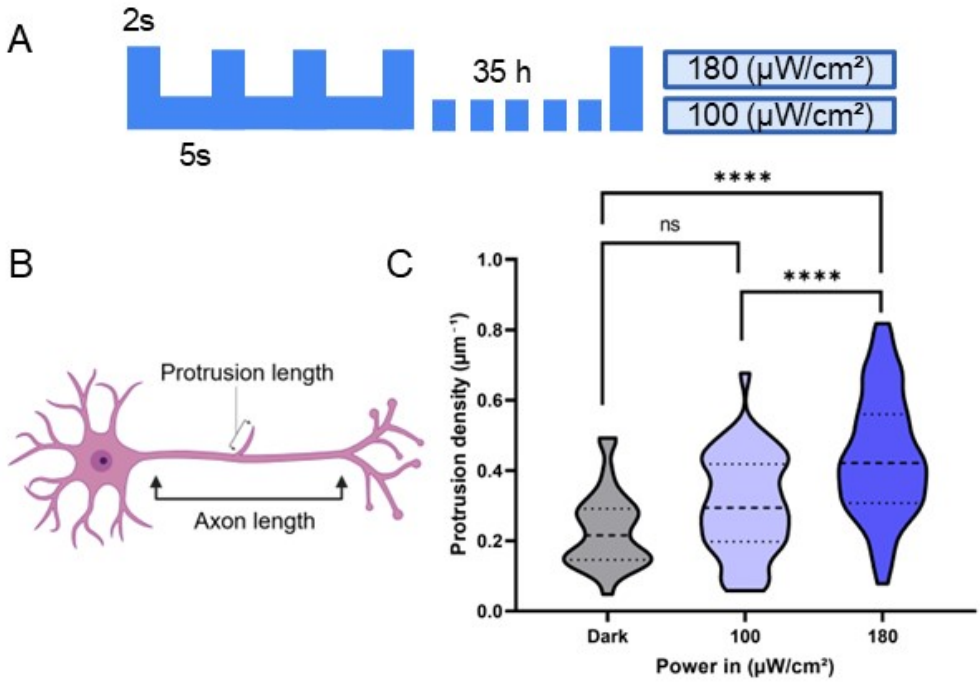

Figure 3.5 Intensity dependent increase in protrusion density in chick spinal neurons transfected with Opto-TrkA. A) Light stimulation module activation for 35 hours with two different light intensities (180 µW/cm² and 100 µW/cm²) compared to dark (no light exposure). B) Schematic of quantification for morphometric analysis. Protrusion density is defined as the number of protrusions divided by the length of the axon. C) Stimulation at 100 µW/cm² did not induce any change in protrusion density, whereas stimulation at 180 µW/cm² resulted in a significant increase in protrusion density compared to both the 100 µW/cm² condition and the control (non-stimulated). Mann-Whitney U test was conducted for

statistical significance ($p < 0.0001$), with n = 49 for 180 μW/cm², n = 46 for 100 μW/cm², and n = 30 for the control.

3.1.4 Optogenetic Activation of Chick Spinal Neurons Using Opto-TrkA and Opto-TrkB

Next, Opto-TrkA and Opto-TrkB transfected were subjected to Arduino-controlled global light stimulation setup. Primary chick embryonic spinal neurons were transfected (electroporated) with Opto-TrkA-mCitrine/Opto-TrkB-mCitrine/pCAG-GFP(control) and plated on poly-D-lysine (PDL)-coated dishes. The cultures were incubated at 37°C for one hour before being transferred to the Arduino-controlled global activation setup, maintained at 37°C. Neurons were subjected to light stimulation for 35 hours, followed by fixation with 4% paraformaldehyde (PFA). For cytoskeletal visualization, neurons were stained with Alexa Fluor 568-conjugated phalloidin, which labels F-actin. With the around 20% transfection efficiency of electroporation, only cells expressing Opto-TrkA-mCitrine /Opto-TrkB-mCitrine/pCAG-GFP(control) were analyzed. Morphometric parameters, including axon shaft length, protrusion length, number of protrusions, protrusion density, and growth cone area, were quantified using the cytoskeletal marker stated above (Fig. 3.4).

Both Opto-TrkA-mCitrine and Opto-TrkB-mCitrine exhibited round, punctate-like vesicles which were mobile (Fig. 3.6 B, D). The expression pattern was consistent with the established Trk receptor signaling. The distribution appeared uniform, with no noticeable polarization. Neurons transfected with Opto-TrkA-mCitrine and Opto-TrkB-mCitrine displayed a significantly higher number of protrusions per unit axon length compared to GFP-transfected control neurons (Fig. 3.7), but no difference was observed between Opto-TrkA and Opto-TrkB. Additionally, no significant differences were observed in axonal protrusion length or axon shaft length (Fig. 3.7). Further, area of the growth cone (measured manually by masking the growth cone region using the segment tool in FIJI IMAGEJ) for Opto-TrkB, was found to be significantly higher than both Opto-TrkA and control GFP transfected neurons (Fig. 3.7).

These results suggest that blue light stimulation (under global activation setup) for 35 hours, resulted in increased filopodial protrusion density in both Opto-TrkA and Opto-TrkB transfected neurons as compared to the control GFP transfected set. Opto-TrkA was further tested for localized stimulation for studying branch formation in chick spinal neurons.

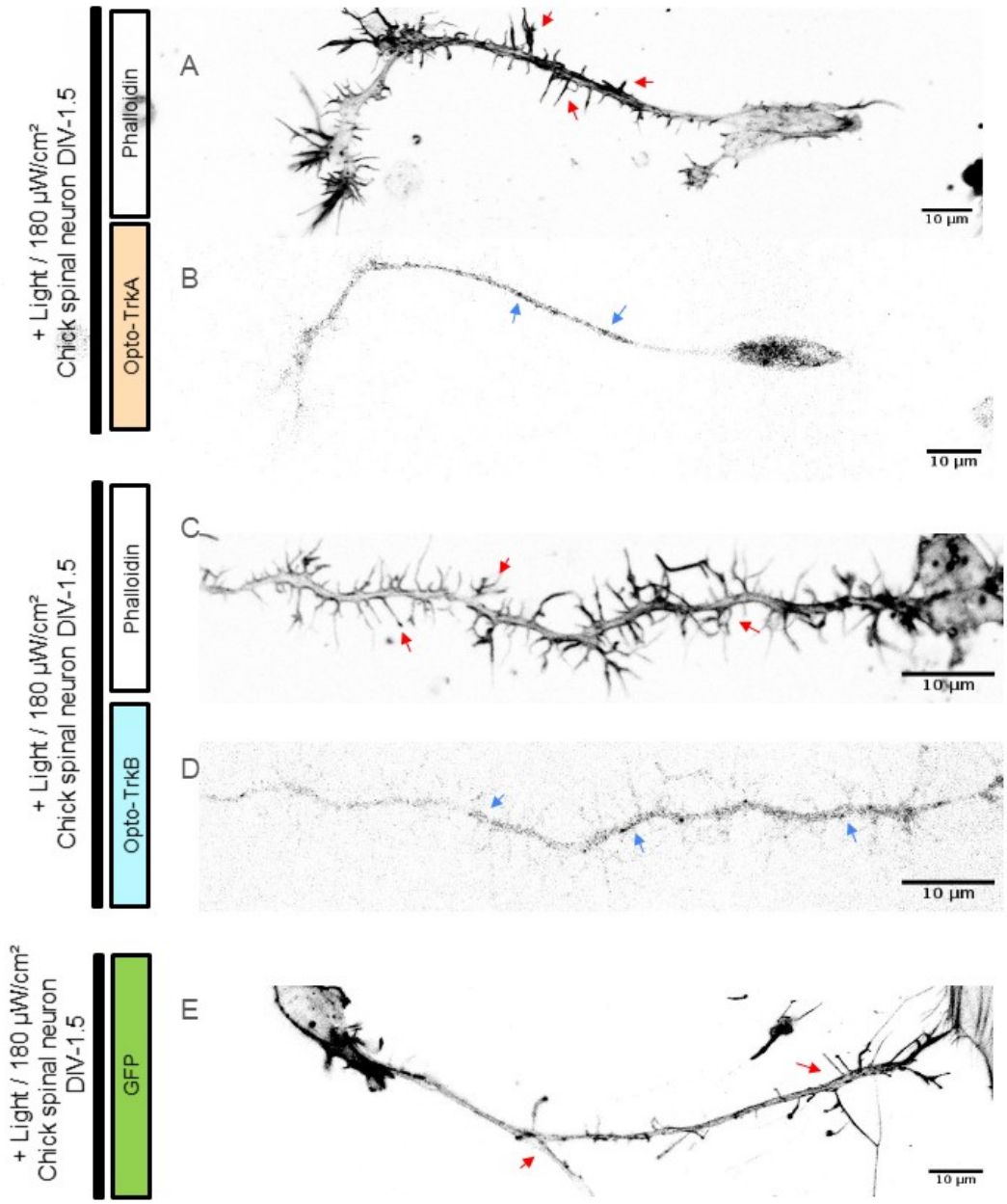

Figure 3.6 Representative micrographs of chick spinal neurons, light stimulated; transfected with Opto-TrkA A) Corresponding phalloidin label B) corresponding Opto-TrkA expression. Similarly, for

Opto-TrkB transfected neuron, C) Corresponding Phalloidin label D) Opto-TrkB expression E) Phalloidin label for GFP transfected (control for optical stimulation). (Phalloidin conjugated with Alexa-568 in all). Red arrows represent collateral protrusions, blue arrows represent punctate expressions of Optro-TrkA and Opto-TrkB Scale - 10 µm, DIV 1.5 - 36 hours post plating.

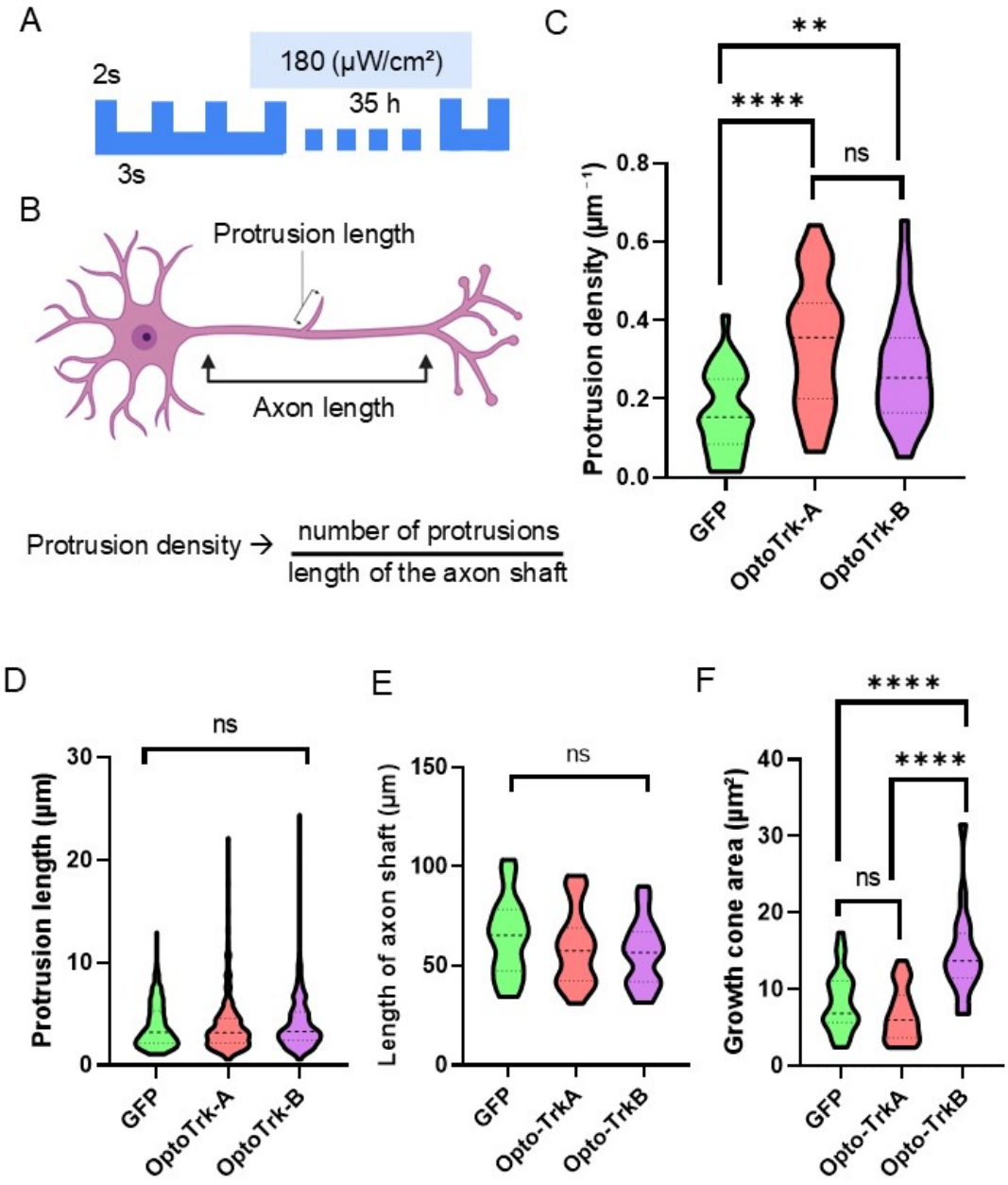

Figure 3.7 A) Light stimulation protocol used in this study. Blue LED light (180 µW/cm²) with on/off cycles of 2 s / 3 s for a total duration of 35 hours. B) Schematic for morphological analysis of the neurons. C) Optical stimulation increases the density of protrusions along the axon shaft in both Opto-TrkA and Opto-TrkB neurons compared to GFP ($p < 0.00001$ for Opto-TrkA vs. GFP; $p < 0.01$ for Opto-TrkB vs. GFP; $n = 29$ for Opto-TrkA, $n = 30$ for Opto-TrkB, and $n = 29$ for GFP). No significant difference was

observed between Opto-TrkA and Opto-TrkB. A Mann-Whitney U test was used to assess statistical differences individually between the sets. D) Protrusion lengths were not significantly different between groups, as determined by individual t-tests and one-way ANOVA ($p > 0.05$). E) No significant differences were observed in axon shaft length among Opto-TrkA, Opto-TrkB, and GFP conditions. Difference in total area of growth cones for the same neurons.

3.1.5 Spatially Controlled Activation of Opto-TrkA in Chick Spinal Neurons

As outlined in Section 1.3, branch formation is a multistep process involving actin patch formation, patch stabilization, protrusion formation, and ultimately, microtubule innervation (Armijo-Weingart and Gallo, 2017). Localized NGF-mediated Trk stimulation has been shown to initiate these changes (Gallo and Letourneau, 1998). Previous studies have employed microfluidic chamber setups to generate localized NGF gradients for investigating neurodevelopment. However, a key limitation of these approaches is the loss of spatial specificity due to NGF diffusion and its minor affinity for other receptors (Jocher et al., 2018, Huang and Reichardt, 2003).

A potential solution to this limitation is the local stimulation of optogenetic Trk receptors, enabling precise spatiotemporal control over receptor activation. For instance, in a recent study, local induction of optogenetic TrkB at the neurite end has been shown to promote neurite elongation (Woo et al., 2019). This approach allows for a targeted investigation of downstream signaling events leading to branch formation.

Based on previous experiments, we conclude that prolonged (35-hour) light stimulation of Opto-TrkA leads to a significant increase in the density of collateral branches along the axon shaft. In this experiment, we aimed to induce branch formation through local activation in chick spinal neurons transfected with Opto-TrkA.

To achieve this, primary chick spinal neurons were co-transfected with Opto-TrkA-mCitrine and F-tractin-mCherry (labels F-actin) and subsequently plated on poly-D-lysine (PDL)-coated dishes. The cultures were incubated at 37°C for 36 hours prior to stimulation. Following incubation, the culture dish was placed in a stage incubator of a confocal imaging system (maintained at 37°C). A co-transfected neuron was then identified for stimulation, with preference given to neurons exhibiting little to no pre-formed branches, as they were ideal to study induced branching (Fig. 3.8).

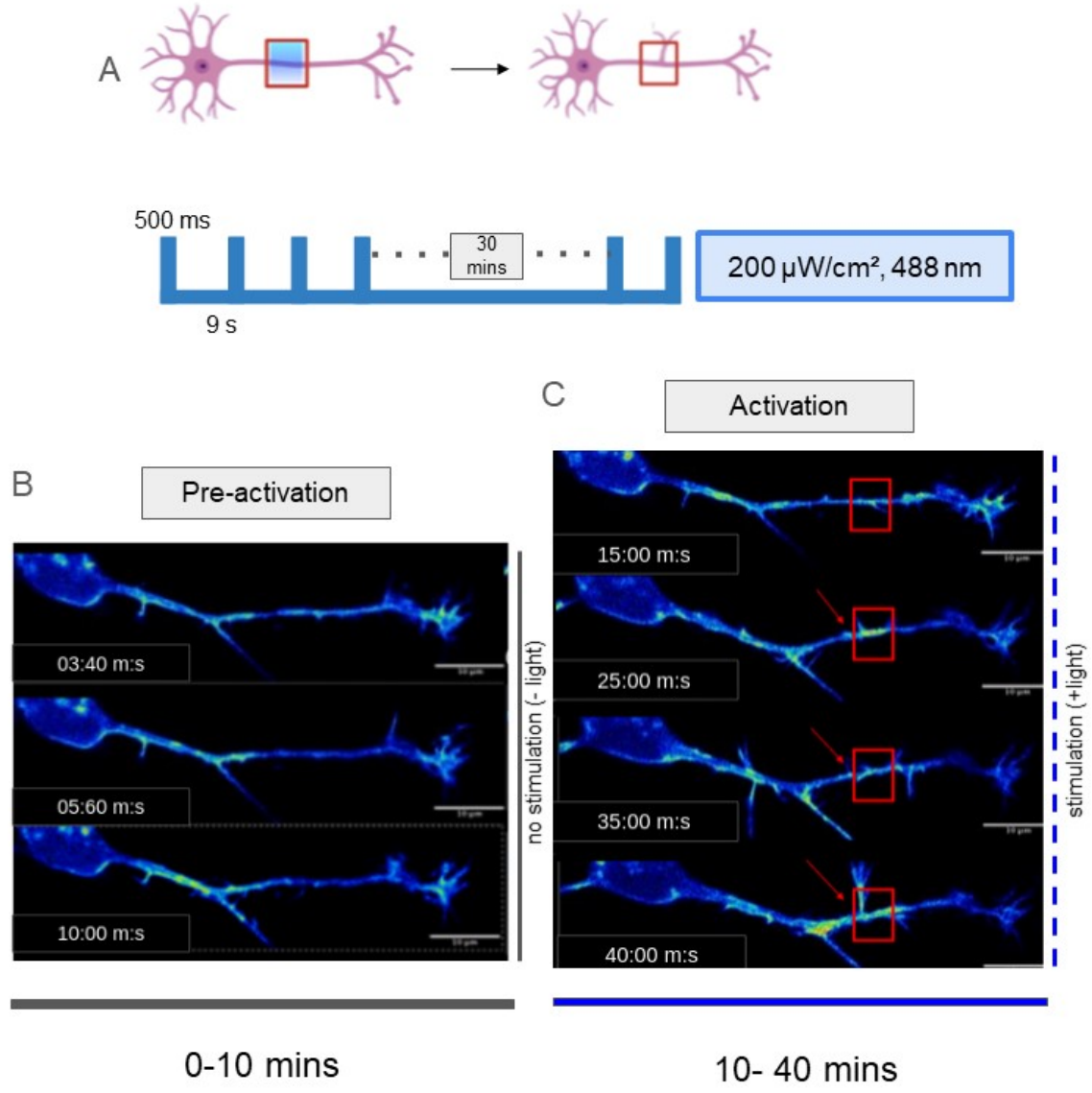

Figure 3.8 A) Schematic representation of the local light stimulation module for chick spinal neurons transfected with Opto-TrkA and F-tractin-mCherry. The region of interest (ROI) is stimulated once every 9 seconds for 500 ms using a 488 nm laser at an intensity of 200 µW/cm². B, C) Representative images of a chick spinal neuron subjected to local activation. The left panel shows the F-tractin channel of the neuron before activation (10 min), while the right panel depicts the neuron after 30 min of activation. The red arrow indicates the emergence of a protrusion at the site of stimulation. A 16-color intensity LUT filter (Fiji) was applied; the blue region represents low intensity, while the green-yellow region indicates high F-actin intensity. Scale bar: 10 µm. Created in https://BioRender.com

Baseline (pre-activation) imaging was conducted in the F-tractin channel for 10 minutes, with images acquired every 10 seconds. Based on this pre-stimulation, a region of interest (ROI) was selected, ensuring minimal protrusive activity prior to induction. The designated ROI was then subjected to activation using the 488 nm laser (200 μW/cm²), at a 60X objective. The ROI was stimulated once every 9 seconds, with the F-tractin-mCherry channel imaged at the same frequency. This cycle continued for 30 minutes, during which the selected ROI underwent multiple stimulations as per the specified protocol.

Further, F-actin intensity changes were assessed using Ftractin-mCherry across three distinct regions of interest (ROIs). The central ROI (blue) corresponded to the stimulation site, while the left (red) and right (yellow) control ROIs were positioned on either side of the stimulated region (Fig. 3.10).

Neuron	1	2	3	4	5	6	7	8	9	10	11	12	13
Pre-activation	✓	✓	X	X	✓	✓	✓	X	X	✓	X	X	X
Activation	✓	✓	✓	✓	✓	✓	✓	✓	✓	✓	X	✓	X

New filopodia Pre-existing filopodia No filopodia even after stimulation

Figure 3.9 The table represents a binary presentation (✅ - protrusion found, ❌ - protrusion absent) at the region of interest (ROI) during the pre-activation (10 min) and activation (30 min) phases for the 13 chick spinal neurons.

Out of the 13 sets of neurons analyzed, 11 exhibited filopodial protrusion formation following local optogenetic stimulation (Fig. 3.9). However, 6 of the 13 neurons (1, 2, 5, 6, 7, 10) displayed some degree of pre-existing filopodial activity in the marked ROI during the 10-minute control acquisition prior to stimulation. In contrast, 5 neurons (3, 4, 8, 9, 12) that initially lacked protrusive activity in the control set developed filopodia following stimulation. Meanwhile, 2 neurons (11, 13) exhibited no filopodial activity either before or after stimulation. Collectively, only 5 out of the 13 neurons successfully resulted in a formation of filopodia.

Interestingly, in the 6 neurons with pre-existing filopodial activity, 5 displayed highly transient protrusions that typically collapsed within 20–30 seconds. Upon optogenetic stimulation, however, these protrusions appeared more stable, persisting for longer durations before collapsing. Furthermore, many of these neurons exhibited increased local protrusive activity, characterized by multiple filopodia forming and collapsing dynamically within the stimulation region.

Despite the formation of filopodia during stimulation, most protrusions were transient and eventually collapsed or shifted within a few minutes. These findings suggest that while some neurons exhibit basal filopodial activity, optogenetic stimulation enhances both the stability and frequency of filopodial protrusions. However, in contrast to prolonged global activation (Section 3.6), which led to robust increase in protrusion density, the stimulation protocol used in this experiment might not have been sufficient to induce stable protrusions. This underscores the possibility that more frequent or prolonged stimulation bouts may be required to facilitate sustained activation for branching.

3.1.6 F-actin Intensity Following Opto-TrkA Stimulation in Chick Spinal Neurons

Interestingly, in 8 neurons (2,3,4,5,6,8,10), a local increase in F-actin density was observed in the region of stimulation. This increase in Factin pool was seen to be associated with decrease in Factin from the surrounding ROI in some cases. Additionally, this increase in Factin intensity was observed at slightly different time points across the different neurons; roughly after 15 minutes of stimulation, although in 4 cases, the change was observed after 5 minutes of stimulation.

Collectively, while local stimulation of Opto TrkA in chick spinal neurons induce some filopodial activity, taking the 13 neurons into account, the light stimulation frequency most probably stands inefficient in initiating filopodia formation in a regulated and controlled manner. Secondly, chick spinal neurons were observed to have a very high base line of branching, with transient protrusive activity throughout the axonal shaft. This can be noticed from the fluctuations in integrated density plots provided (Fig. 3.11). Moreover, the inconsistencies in the observation can be partially accounted by the

heterogenous neuronal population in the chick spinal neurons. Although all of the 13 neurons were stimulated at 36 hour post plating, different levels of basal branching dynamicity were observed in most of the cases. This necessitates a better model system which would have a very low baseline for branching. Therefore I shifted to chick DRG (Dorsal Root Ganglion) neurons because of the homogeneous cell population and low base line of branching.

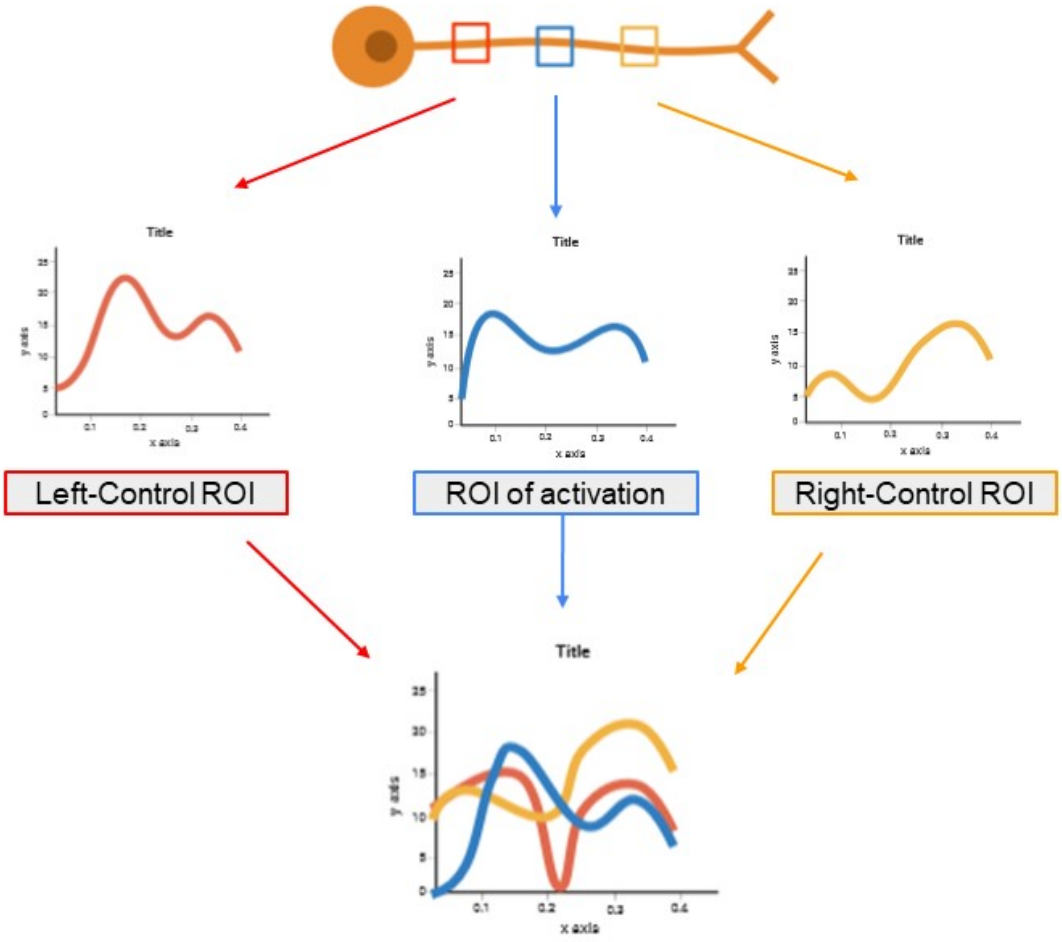

Figure 3.10 Schematic of integrated density plots to understand change in actin intensity upon light stimulation at the center ROI. Blue lines represent the ROI of stimulation, ROI left to stimulation site, Yellow- ROI right to stimulation site. Plots from 3 of the ROI are clubbed with the same time point for better qualitative understanding. Created in https://BioRender.com

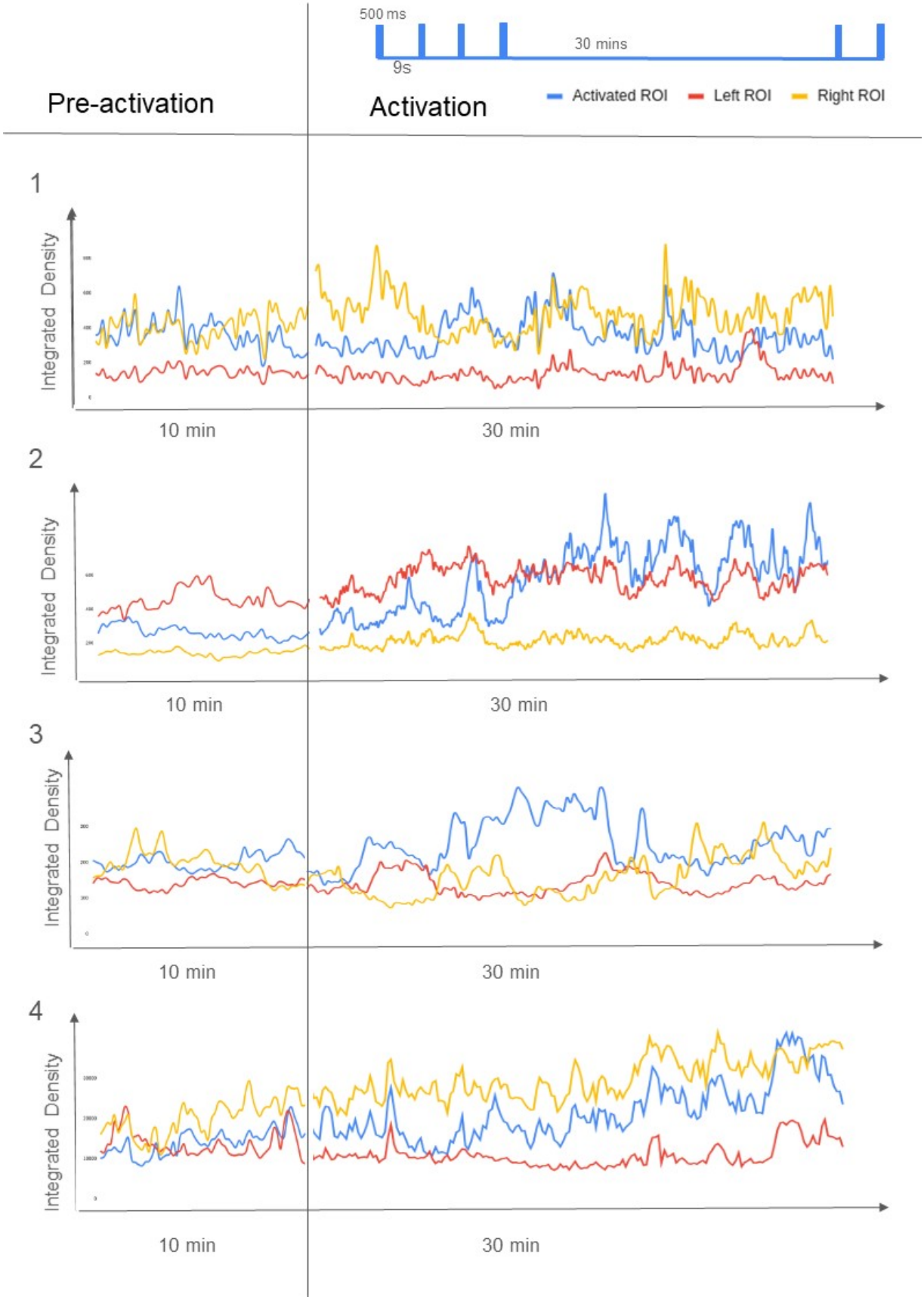
500 ms
30 mins
9s
Activated ROI
Left ROI
Right ROI
Pre-activation
Activation
1
2
3
4
Integrated Density
10 min
30 min

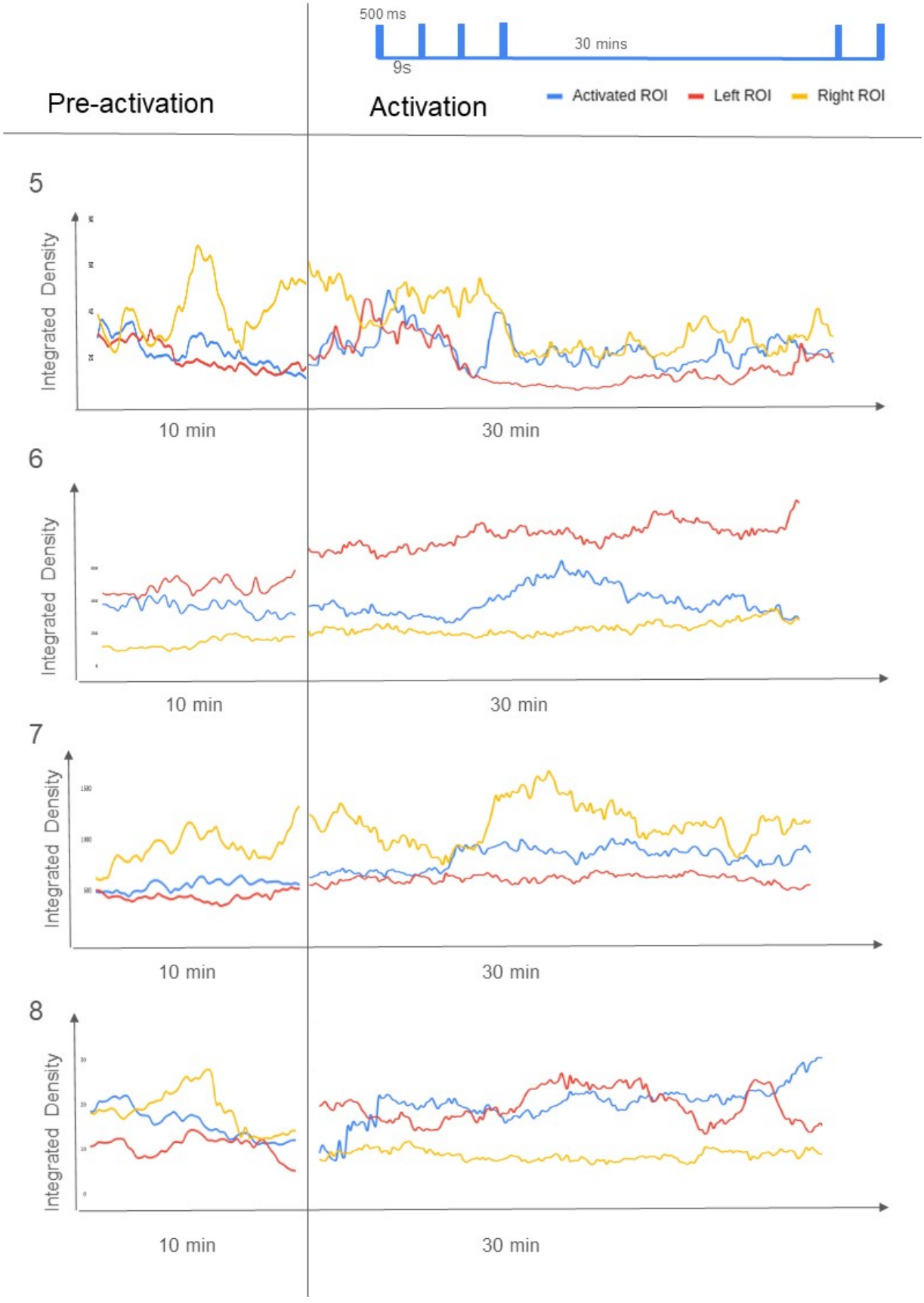
500 ms
30 mins
9s
Activated ROI
Left ROI
Right ROI
Pre-activation
Activation
5
Integrated Density
10 min
30 min
6
Integrated Density
10 min
30 min
7
Integrated Density
10 min
30 min
8
Integrated Density
10 min
30 min

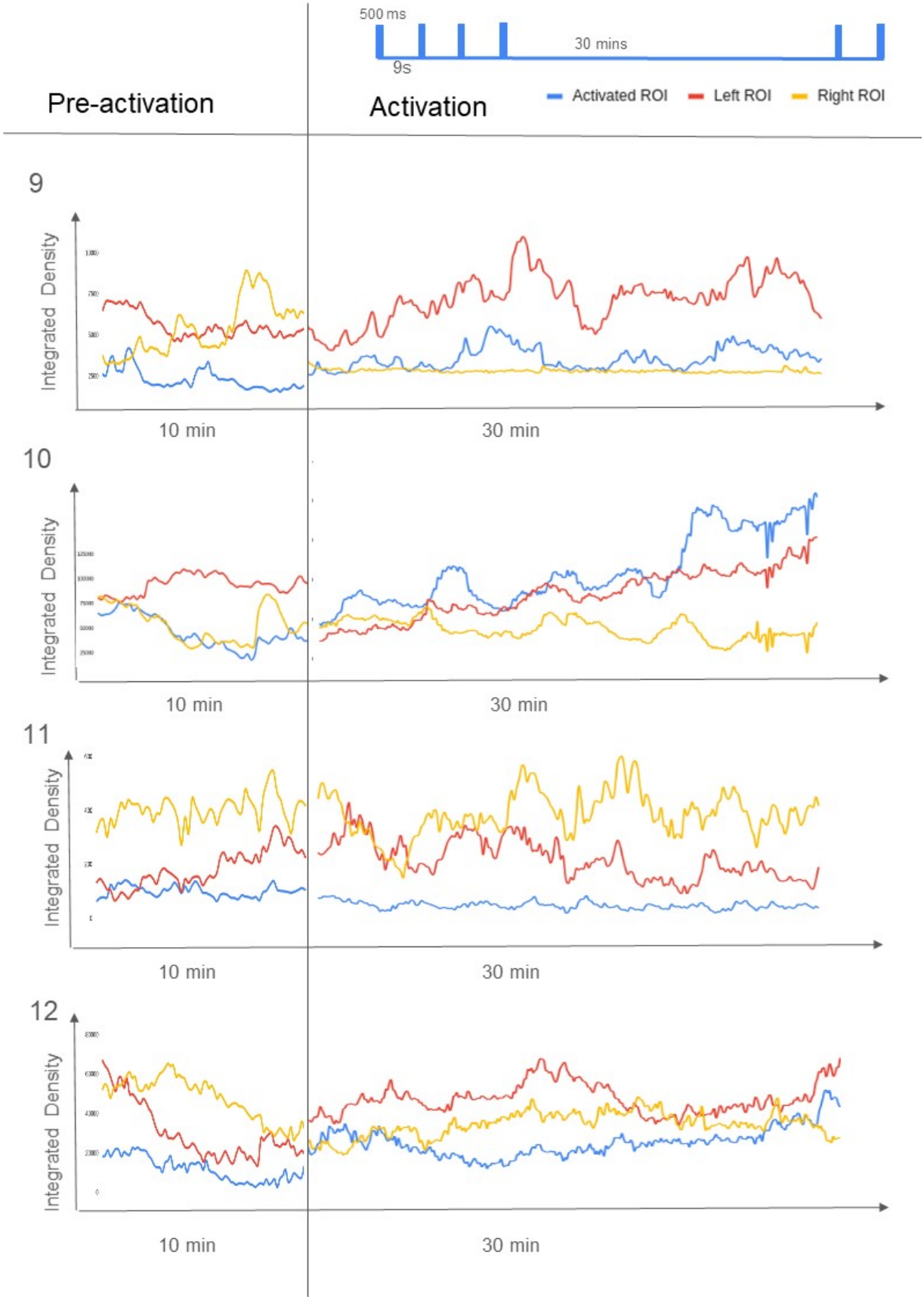
500 ms
30 mins
9s
Activated ROI
Left ROI
Right ROI
Pre-activation
Activation
9
10
11
12
Integrated Density
10 min
30 min

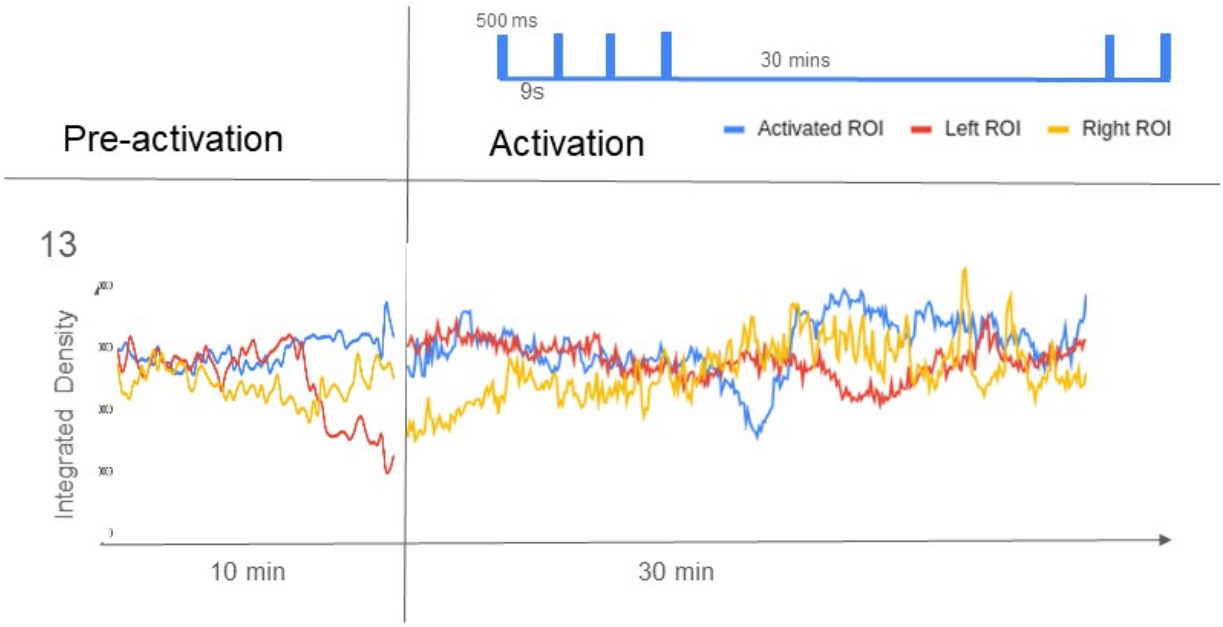

Figure 3.11 Above graphs represent integrated density plots for the 13 chick spinal neurons to study changes in F-actin intensity upon local activation in the ROI of stimulation, compared to two neighbouring non-stimulated ROI. Numbers in the left margin represent each of the 13 neurons that are discussed in Figure 3.9 (table). Blue lines represent the ROI of stimulation, ROI left to stimulation site, Yellow- ROI right to stimulation site.

3.1.7 Optogenetic Activation of Chick DRG Neurons Using Opto-TrkA and Opto-TrkB

As with spinal neurons, DRG neurons transfected with Opto-TrkA/Opto-TrkB were subjected to global activation setup to study their protrusion-formation efficiency.

Primary chick embryonic DRG neurons were transfected (electroporated) with Opto -TrkA-mCitrine/Opto-TrkB-mCitrine/pCAG-GFP(control)/Opto-TrkB-Y515F-mCitrine(control) and plated on poly-D-lysine (PDL)-coated dishes. The Opto-TrkB-Y515F-mCitrine construct carries a point mutation (Y515F), which disrupts autophosphorylation at Y515 in the intracellular domain, resulting in the failure in recruitment of key effector protein recruitment (like Shc - Src homology 2 domain-containing protein), which further inhibits activation of both PI3K/Akt and MAPK/ERK pathways (Woo et al., 2019). The cultures were incubated at 37°C for one hour before being transferred to the

Arduino-controlled global activation setup, maintained at 37°C. Neurons were subjected to blue light stimulation for 35 hours, followed by fixation with 4% paraformaldehyde (PFA). For cytoskeletal visualization, neurons were stained with Alexa Fluor 568-conjugated phalloidin, which labels F-actin. Given the ~20% transfection efficiency of electroporation, only cells expressing Opto-TrkA-mCitrine/Opto-TrkB-mCitrine/pCAG-GFP(control)/Opto-TrkB-Y515F-mCitrine (control) were analyzed. Morphometric parameters, including axon shaft length, protrusion length, number of protrusions, and protrusion density, were quantified using the cytoskeleton marker mentioned above.

Interestingly, a significant increase in protrusion density was observed in Opto-TrkA transfected neurons. Similarly, Opto-TrkB transfected neurons exhibited a substantial increase in protrusion density compared to both control groups (GFP and Opto-TrkB-Y515F) (Fig. 3.13). Compared to chick spinal neurons, the basal level of branching in chick DRG neurons was significantly lower (Fig. 3.13), as assessed by the protrusion density of GFP transfected cells, which served as a control. However, as observed in spinal cultures, no changes were detected in axon shaft length or protrusion length. This observation contrasts with previous studies in which neurons were cultured in NGF- and BDNF-stimulated environments (Daniel G. Gibson et al., 2011;Kellner et al., 2014)). These results suggest that prolonged (35 hours) global activation enhances filopodial protrusion density in both Opto-TrkA and Opto-TrkB transfected neurons compared to the control (GFP and Opto-TrkB-Y515F transfected neurons). Further, they are currently being tested under local activation setup for branch formation at the point of stimulation.

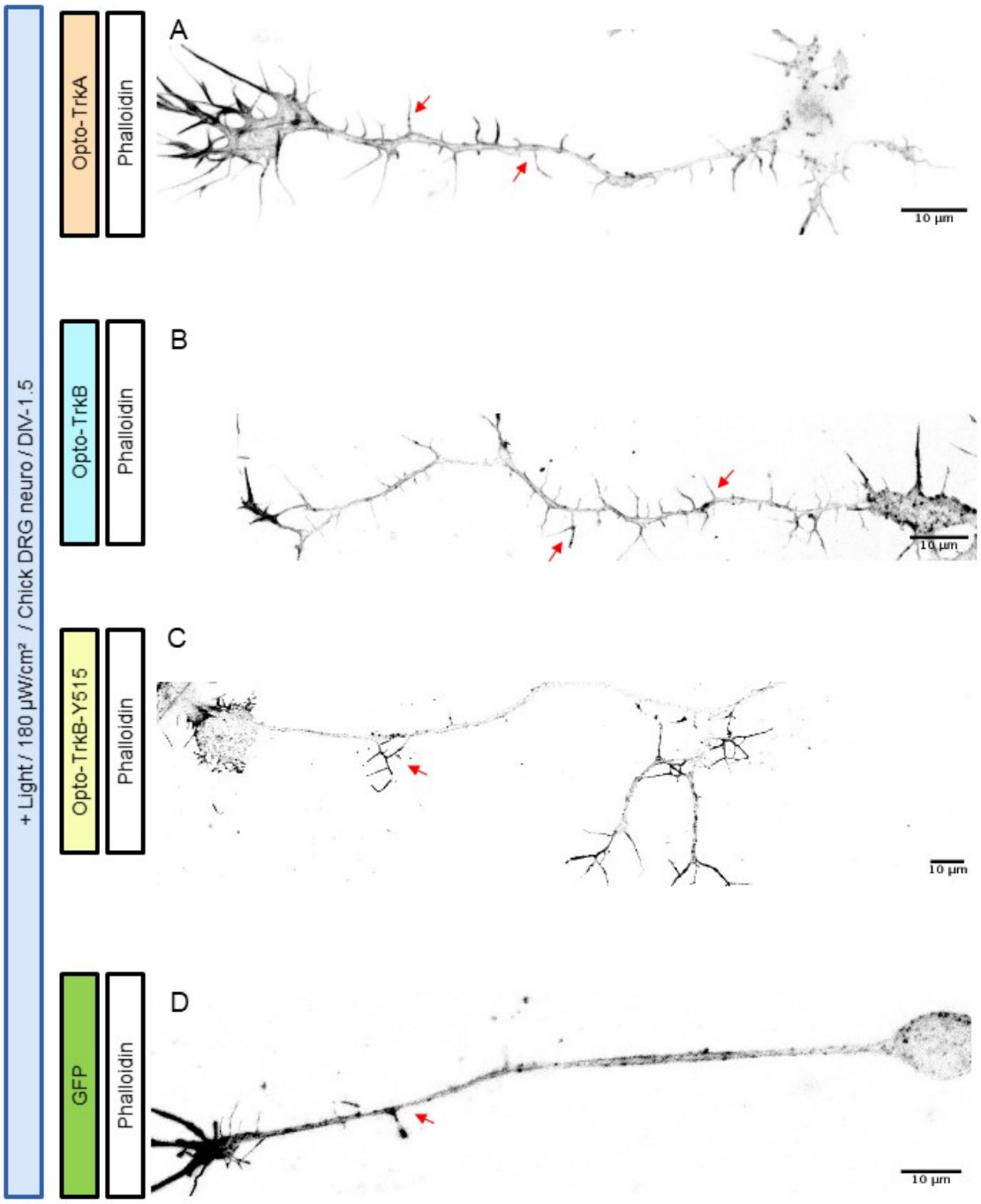

Figure 3.12 Representative micrographs of light-stimulated chick DRG neurons stained with phalloidin (conjugated with Alexa568). Neuron transfected with A) Opto-TrkA, B) Opto-TrkB, C) Opto-TrkB-Y515F, D) GFP. Scale bar: 10 µm. DIV I.5 – 36 hours post plating. Red arrows represent collateral protrusions.

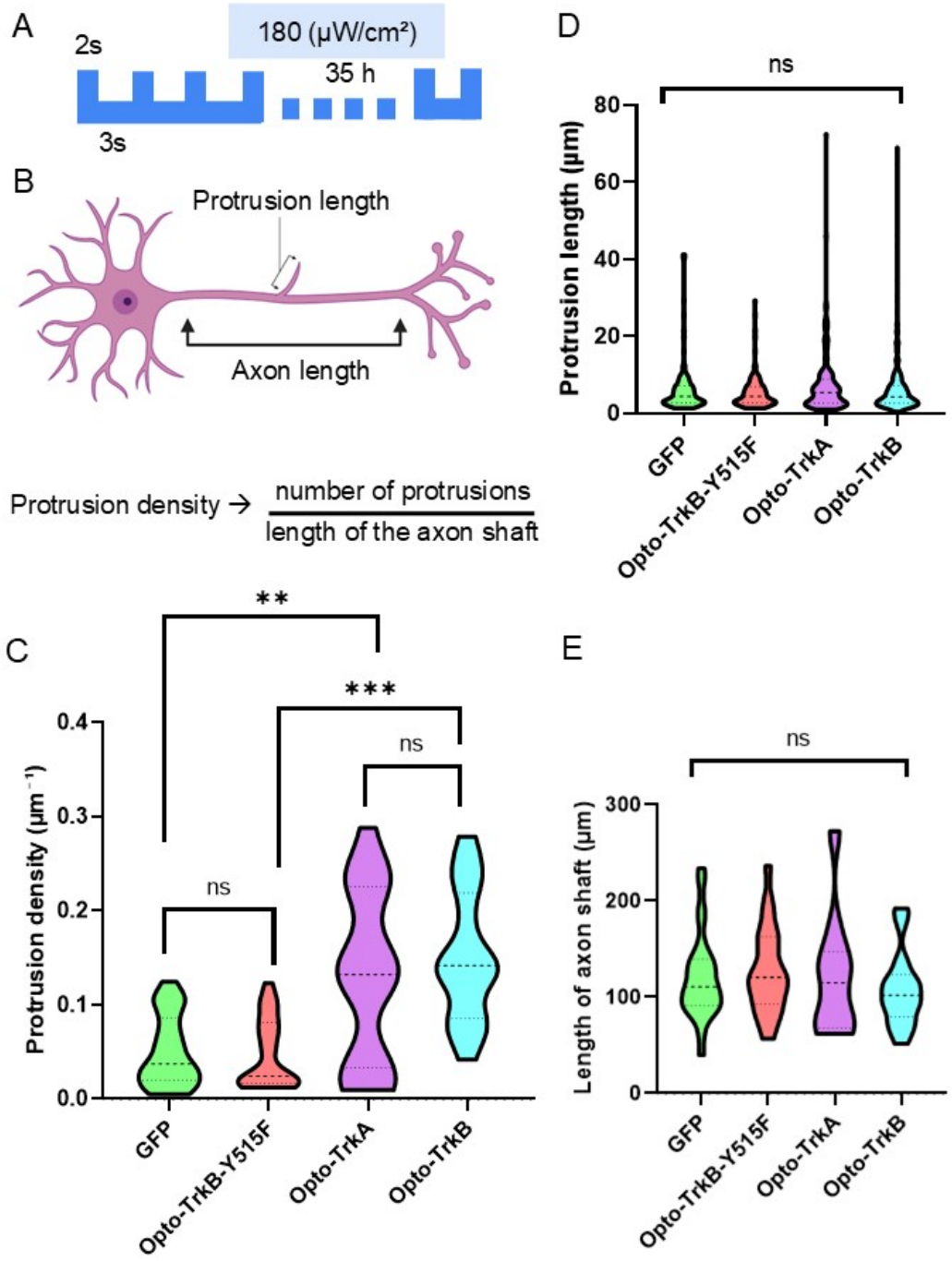

Figure 3.13 A) Light stimulation protocol used in this study. Blue LED light (180 W) used with an ON/OFF cycle of 2 s / 3 s for a total duration of 35 hours. B) Schematic for morphological analysis of the neurons. C) Opto-TrkB exhibited significantly higher protrusion density compared to Opto-TrkB-Y515F ($P < 0.0001$). Opto-TrkA showed a significantly higher protrusion density compared to GFP (**$P = 0.0032$). No significant difference was observed between Opto-TrkA and Opto-TrkB or between GFP and

Opto-TrkB-Y515F (ns). Sample sizes are as follows: Opto-TrkA (n = 28, N = 3), Opto-TrkB (n = 33, N = 3), Opto-TrkB-Y515F (n = 31, N = 3), and GFP (n = 21, N = 2). D) Length of protrusions. Statistical significance was assessed using the Mann-Whitney U test. No significant differences were observed between any of the conditions (ns). Sample sizes are as follows: Opto-TrkA (n = 140), Opto-TrkB (n = 325), Opto-TrkB-Y515F (n = 100), and GFP (n = 143). E) Statistical comparisons were performed using the Mann-Whitney U test. No significant differences were observed between any conditions (ns). Sample sizes: Opto-TrkA (n = 28, N = 3), Opto-TrkB (n = 33, N = 3), Opto-TrkB-Y515F (n = 31, N = 3), and GFP (n = 21, N = 2).

3.4. Eps8 Knockdown: Promoting Stable Branches or Transient Extensions

Axonal collateral branching is a highly dynamic process that requires the synchronized association of various effector proteins for its active regulation. As discussed previously, local actin hotspots serve as precursors for the formation of protrusions. Actin-binding proteins that regulate polymerization, depolymerization, and capping are locally recruited to these hotspots, thereby regulating the transition from hotspot formation to protrusion development or complete dissociation (Armijo-Weingart and Gallo, 2017).

One such cytoskeletal regulatory protein is Eps8, an actin-binding protein involved in cytoskeletal remodeling. Eps8 modulates actin dynamics by binding to actin filaments and inhibiting their polymerization and growth. As per previous work from our lab, overexpression of Eps8 in chick spinal neurons results in a decreased protrusion density , whereas knockdown via splice-blocking morpholino (SBMO) transfection leads to an increased protrusion density compared to GFP (control) transfected neurons (Pagrut, 2023).

Prior studies have demonstrated that branch maturation is often associated with the invasion of microtubules, a critical step in branch stabilization (Gallo, 2011; Tymanskyj et al., 2017). However, it remains unclear whether the increased number of branches observed upon Eps8 knockdown mature to stable branches. Further investigation is required to elucidate whether the increased protrusion density observed under Eps8 knockdown conditions further matures to stable protrusions with microtubule innervation.

To address this, I transfected chick spinal neurons with Eps8 splice-blocking morpholino (SBMO) and subsequently labelled microtubule organization using β3-tubulin immunostaining alongside Alexa Fluor 568-conjugated phalloidin labelling. Through morphological analysis, I aimed to quantify the proportion of protrusions containing microtubules. But before using morpholino for knockdown, successful validation of knock down efficiency of morpholino was required.

3.4.1 RT-PCR based Eps8 knockdown efficiency assessment

Among the various methodologies employed for gene knockdown, splice-blocking morpholinos (SBMO) are widely used due to their ability to modulate RNA processing. These morpholinos exhibit high affinity for specific regions of pre-mRNA, disrupting the splicing process. This mechanism highlights their effectiveness in validating gene knockdown strategies.

Binding of SBMO to a target sequence in the pre-mRNA, prevents the proper recruitment of the splicing machinery at exon-intron junctions. As a result, the spliceosome complex fails to correctly excise introns, leading to splicing anomalies such as intron retention or exon skipping (Fig. 3.14). The mis-spliced mRNA is highly susceptible to frameshift mutations, premature stop codons, or the formation of aberrant secondary structures. These defects may impair translation efficiency or lead to degradation of the transcript before translation, ultimately resulting in the production of a truncated protein. The Eps8 splice-blocking morpholino binds to the junction between exon 9 and the following intron of the *Eps8* gene, as shown in the schematic (Fig. 3.14). This results in intron retention during splicing. RT-PCR (Reverse Transcription Polymerase Chain Reaction) of *Eps8* SBMO-transfected neurons can help assess these mis-spliced variants. The forward primer is designed to bind within exon 8, while the reverse primer binds within exon 10. The wild-type band is thus expected to be approximately 230 bp, whereas the intron-retained variant should produce a band of 1990 bp.

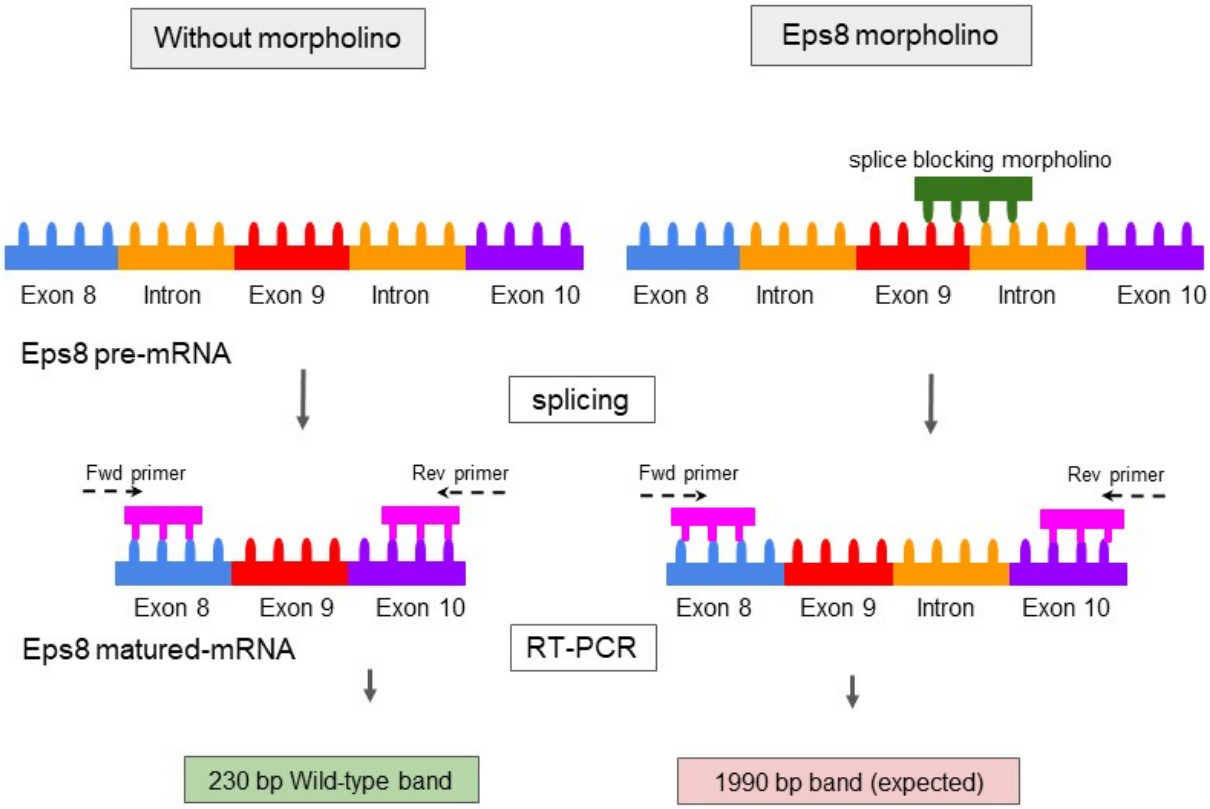

Figure 3.14 Schematic of the Eps8 splice-blocking morpholino (SBMO) binding between exon 9 and the adjacent intron of the Eps8 gene, resulting in intron retention in the spliced mRNA. The forward primer is designed to bind exon 8, while the reverse primer binds exon 10 of the spliced mRNA. This generates a 230 bp wild-type band, whereas the SBMO-induced mis-spliced transcript produces a 1990 bp band, both of which can be detected via RT-PCR.

Neurons were seeded in four (20 mm) cell culture-treated dishes, each coated with 75 µg/mL poly-D-lysine (PDL) solution. The cultures were prepared using spinal tissue obtained from two eggs, corresponding to approximately one and a half spinal cords. For transfection, 10 µL of either splice-blocking (SBMO)/control morpholino (CMO) was mixed with 90 µL of Opti-MEM. RNA isolation from primary spinal neuron cultures was performed using a column-based purification method. After RNA extraction, cDNA synthesis was performed according to the protocol outlined in the Materials and Methods section. A PCR assay was then performed to amplify the region of interest (exons 8, 9, and 10). Based on the expected splicing outcomes, a 2kb band is expected (with intron retention)(Fig. 3.15).

Interestingly, in the splice-blocking morpholino set, multiple additional bands were observed compared to the control morpholino (CMO). Apart from the expected 2 kb band (indicative of intron inclusion), additional bands were observed, possibly resulting from alternative splicing events. Since electroporation does not achieve 100% transfection efficiency, the SBMO-transfected population also contained a significant fraction of the wild-type spliced product, which was 230 bp).

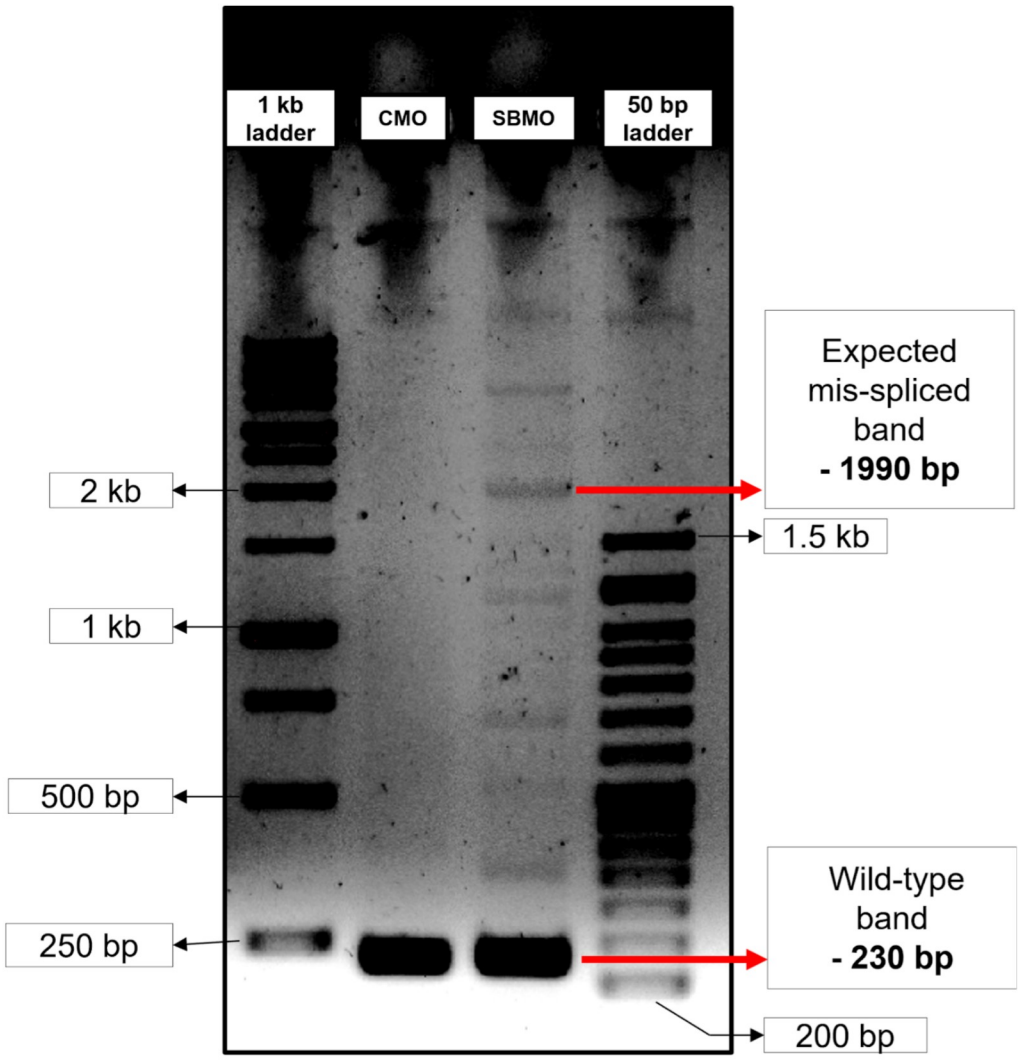

Figure 3.15 Agarose gel electrophoresis (1%) showing RT-PCR products for control morpholino (CMO) and splice-blocking morpholino (SBMO), to visualize splice variants. Lane left to CMO is a 1kb ladder while right to SBMO is a 50 bp ladder. The red arrow indicates wild-type band and the expected intron included splice variant. Other mis-spliced products resulting from *Eps8* SBMO treatment can also be observed in the SBMO lane, which is absent in the CMO lane.

3.4.2 Elevated Mature Protrusions in Neurons Upon Eps8 Knockdown

Microtubule invasion is often considered to be a late event, reflective of maturation of collateral protrusions into stable branches. Based on the observations from the previous experiment, Eps8 splice-blocking morpholino (SBMO) was used to knock down Eps8 in neurons and quantify the percentage of branches exhibiting Eps8-dependent microtubule invasion. Chick spinal neurons were transfected with Eps8 SBMO and GFP and plated on PDL-coated dishes, followed by incubation (37°C) for 72 hours post plating. At this time point, chick spinal neurons usually develop stable branches. The cultures were then fixed using 4% paraformaldehyde (PFA) and stained with Alexa Fluor 568-conjugated phalloidin to label F-actin and β3-tubulin, which was detected using an Alexa Fluor 647–tagged secondary antibody.

Since morpholinos are not fluorescently labeled, pCAG-GFP was co-transfected to visualize transfected neurons. Given that pCAG-GFP (~5 kb) is significantly larger than morpholino oligonucleotides, only neurons expressing GFP were quantified as a qualitative indicator of morpholino transfection. As a control set, neurons were transfected with control morpholino (CMO) and GFP.

Microtubules were visualized using β3-tubulin staining, while Alexa Fluor 568-conjugated phalloidin labeled the overall cytoskeletal structure, marking all protrusions. Nascent and immature protrusions are expected to lack microtubule invasion, whereas most stable branches should contain microtubules (Fig. 3.16). The fraction of microtubule-positive branches was found to be significantly higher in splice-blocking morpholino (SBMO)-transfected cells (Fig. 3.17), suggesting that the increased branching observed upon Eps8 knockdown progresses into stable branch formation. Interestingly, protrusions in the SBMO condition were slightly shorter (Fig. 3.17). Eps8 functions as a capping protein, where its overexpression reduces patch lifetime and protrusion density, while knockdown has the opposite effect (Pagrut, 2023). Given that microtubules invade only a subset of branches while others collapse, the observed increase in microtubule-containing branches may result from an overall rise in total branch formation due to enhanced protrusivity following Eps8 knockdown. The

decrease in protrusion length in the first plot may be accounted to the change in cytoskeletal dynamics due to varied protrusivity in the two cases.

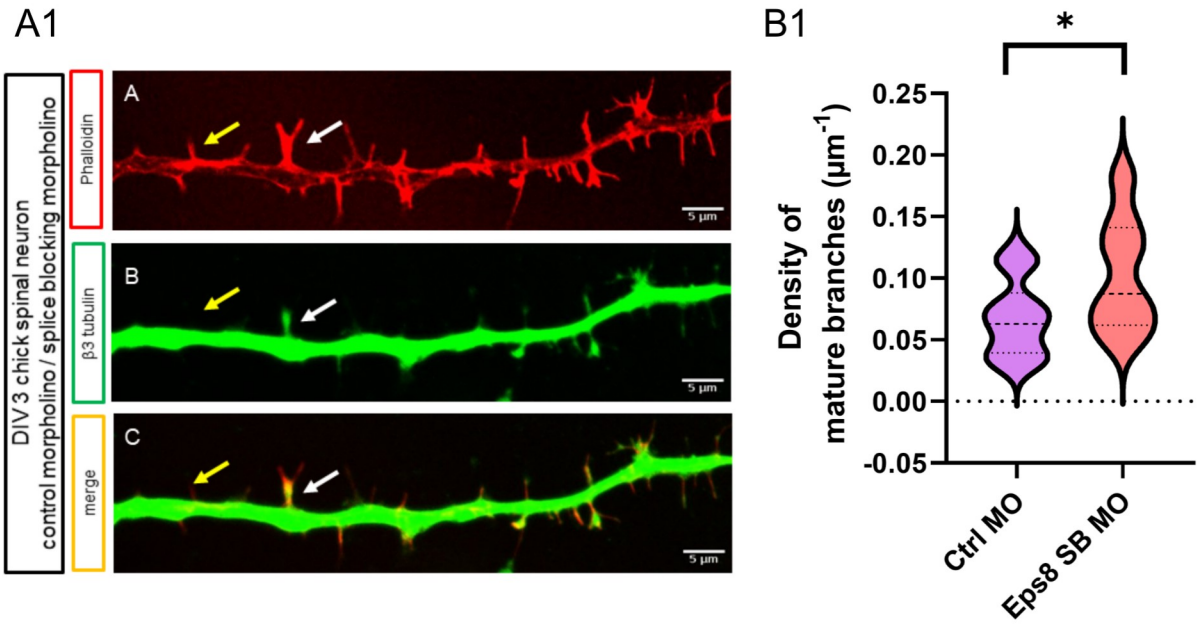

Figure 3.16 A1) Representative micrographs of a segment of an axon having early and mature protrusions (transfected with an Eps8 splice-blocking morpholino/control morpholino), visualized in three different labels A) Phalloidin (conjugated with Alexa568), B) β3-Tubulin, C) Merged micrograph. Yellow arrow indicates a protrusion devoid of microtubule innervation, while white arrow represents a mature protrusion having microtubule invasion. Scale bar: 5 µm. DIV3 – 72 hours post plating. B1) Violin plot showing an increase in the percentage of branches with microtubules in the *Eps8* SBMO condition compared to CMO. Mann-Whitney U test was conducted to test for significance (n = 26 for SBMO, n = 28 for CMO, $p < 0.05$).

Chapter 4 Discussions

In this study, I aimed to develop an optogenetic approach to investigate collateral branching in chick spinal and DRG neurons. I found that prolonged light stimulation led to a significant increase in protrusion density. While previous studies explored collateral branching using NGF- and BDNF-enriched environments, certain technical limitations remained unresolved. For instance, ligand concentrations gradually diminish over time due to oxidation and proteolytic degradation in the external medium. Additionally, NGF is known to bind $p75^{NTR}$, and the resulting downstream signaling varies depending on the specific receptor combinations that dimerize locally (Huang and Reichardt, 2003). My approach establishes a precise and systematic correlation between TrkA and TrkB activation and branch formation within a constitutive light-dependent environment, using two neuronal subtypes with distinct baseline branching patterns.

Although existing literature highlights an increase in axon shaft length in presence of NGF and BDNF, my analysis does not show any change in length of the axons (Fornaro et al., 2020). This can be interpreted in three ways. The first one being, NGF might have a different binding kinetics which is not recapitulated in global activation setup. The second one being, NGF may indirectly associate with other receptors and factors that might not occur in the controlled optogenetic TrkA activation. The last explanation which is likely the most plausible, TrkA receptors might need a gradient of activation in order to result in more directed growth and thereby enhanced extension of axon shafts. As Trk receptors naturally exhibit a more polarized distribution (Karlsson et al., 1998), in the case of overexpressed optogenetic Trk constructs, polarization is minimal or absent, leading to non-differential and uniform activation throughout the neuron. Similarly, no change was observed in protrusion lengths.

Previous studies have highlighted the role of BDNF-TrkB interactions in modulating synaptic connections (Gehler et al., 2004). In this thesis, Opto-TrkB activation in chick spinal neurons resulted in a significant expansion of the growth cone area, which was notably larger than both the control group (GFP-transfected) and the Opto-TrkA activated set. This expansion may be attributed to the activation of downstream signaling pathways that regulate actin cytoskeleton remodeling, facilitating precise

synapse formation at target sites. Further studies are needed to delineate the specific signaling mechanisms underlying this phenotype and to determine its functional significance. Global activation of chick DRG neurons transfected with Opto-TrkA and Opto-TrkB yielded increased filopodial protrusion densities in both Opto-TrkA and Opto-TrkB transfected neurons as compared to the control GFP and Opto-TrkB-Y515F transfected sets. The Y515F point mutation in Opto-TrkB disrupts autophosphorylation at Y515 in the intracellular domain, resulting in the failure in recruitment of key effector protein recruitment. This, in turn, impairs PI3K/Akt and MAPK/ERK signaling and prevents the increase in protrusion density observed with wild-type Opto-TrkB activation. This suggests that one or both of these pathways play a critical role in TrkB-mediated protrusion formation. Given that PI3K/Akt is associated with cytoskeletal reorganization and MAPK/ERK with neuronal growth and differentiation, our findings align with previous studies emphasizing their role in neurite outgrowth (Woo et al., 2019). Additionally, the lack of response in the Y515F mutant, despite intact PLCγ signaling, further highlights the importance of PI3K/Akt and MAPK/ERK pathways in TrkB-induced protrusive growth. However, as observed in spinal and DRG neurons, no significant change was observed with the axonal shaft length and protrusion length. The possible explanations for this remain consistent with those provided for spinal neurons.

Local activation of Opto-TrkA-mCitrine in chick spinal neurons appeared to induce branch formation and protrusive activity. Among 13 neurons analyzed, 11 exhibited protrusions; however, 6 of these displayed some level of protrusive activity during the 10-minute control acquisition. While branches formed upon stimulation were sustained for 5–10 minutes, they ultimately collapsed. In 8 of the cases, stimulation led to a localized accumulation of F-actin at the region of interest (ROI), often accompanied by a decrease in F-actin levels in surrounding areas. A similar redistribution of actin was reported in a previous study where Opto-TrkB-mCitrine was activated in developing neurites (Woo et al., 2019). Additionally, actin blobs have been also observed at branch formation sites in dendrites, though the exact mechanism behind this localization remains unclear (Nithianandam & Chien, 2018), warranting further investigation. Despite some protrusion formation following Opto-TrkA activation, current stimulation parameter stands inefficient to induce a collateral branch. Chick spinal neurons exhibit a

high baseline level of branching, which complicates simulation-based experiments. Effective localized activity requires an accumulation of branch-promoting factors at the stimulated region while suppressing branching in adjacent areas (Gibson et al., 2011). In a condition where protrusions form and collapse dynamically along the axon shaft, achieving such localized accumulation is challenging. Furthermore, the heterogeneous population of chick embryonic spinal neurons adds to the noise, as different neuronal subtypes exhibit variable responses to trophic factor signaling.

However, given global activation resulted in significant increase in protrusion density, one possible reason for the limited effect of local activation could be insufficient stimulation to induce branch formation. Increasing the stimulation frequency may enhance activation and promote branching. The heterogeneity and high baseline branching in chick spinal neurons were mitigated by switching to chick DRG neurons, which exhibit minimal to no baseline protrusive activity. These neurons are currently being tested in the local activation setup. Recently reported optogenetic constructs can also be explored, particularly those lacking the extracellular domain to minimize noise from endogenous ligand binding. Constructs such as CIB1-GFP-CAAX and CRY2-intracellular domain exhibit more localized activation, as the CAAX domain ensures membrane pre-localization, preventing diffusion into the cytoplasm. In contrast, CRY2 alone remains diffusely present in the cytoplasm, potentially leading to activation at various subcellular locations (Wei Zhang et al., 2022).

Previous studies report that Eps8 overexpression reduces collateral branching, whereas SBMO-based knockdown exhibits the opposite effect. Here, I show an increase in microtubule-invaded branches in chick spinal neurons following SBMO-based *Eps8* knockdown. *Eps8*, a capping protein, regulates patch lifetime and dynamics. Its knockdown disrupts this regulation, leading to increased protrusivity and a higher baseline for transient protrusions (Pagrut, 2023). Since microtubules are associated with stable branch formation (Armijo-Weingart and Gallo, 2017) and invade only a fraction of immature branches, the overall increase in branch number may enhance actin polymerization via proteins like Arp2/3 and Fmn2, thereby promoting additional protrusions. This shift in protrusion density likely contributes to the observed increase in microtubule-invaded branches compared to the control.

In conclusion, optogenetic stimulation of Opto-TrkA and Opto-TrkB in chick spinal and DRG neurons resulted in a significant increase in protrusion density under global activation. Local activation of Opto-TrkA in chick spinal neurons led to protrusion formation; however, the presence of spontaneously formed protrusions in the control (ROI before stimulation) and the heterogeneity of the spinal neuron population made it challenging to distinguish stimulation-specific effects. Using DRG neurons, which show minimal protrusive activity, along with a higher stimulation frequency, may help address this issue.

References

1. Azevedo, F.A.C., Carvalho, L.R.B., Grinberg, L.T., Farfel, J.M., Ferretti, R.E.L., Leite, R.E.P., Filho, W.J., Lent, R., and Herculano-Houzel, S. (2009). Equal numbers of neuronal and nonneuronal cells make the human brain an isometrically scaled-up primate brain. Journal of Comparative Neurology 513, 532–541. https://doi.org/10.1002/cne.21974.
2. Hatten, M.E. (1999). Central nervous system neuronal migration. Annu Rev Neurosci 22, 511–539. https://doi.org/10.1146/annurev.neuro.22.1.511.
3. Gibson, D.A., and Ma, L. (2011). Developmental regulation of axon branching in the vertebrate nervous system. Development 138, 183–195. https://doi.org/10.1242/dev.046441.
4. Wessells, N.K., and Nuttall, R.P. (1978). Normal branching, induced branching, and steering of cultured parasympathetic motor neurons. Exp Cell Res 115, 111–122. https://doi.org/10.1016/0014-4827(78)90408-1.
5. Lykissas, M.G., Batistatou, A.K., Charalabopoulos, K.A., and Beris, A.E. (2007). The Role of Neurotrophins in Axonal Growth, Guidance, and Regeneration. Current Neurovascular Research 4, 143–151. https://doi.org/10.2174/156720207780637216.
6. Gallo, G. (2011). The cytoskeletal and signaling mechanisms of axon collateral branching. Developmental Neurobiology 71, 201–220. https://doi.org/10.1002/dneu.20852.
7. Armijo-Weingart, L., and Gallo, G. (2017). It Takes a Village to Raise a Branch: Cellular Mechanisms of the Initiation of Axon Collateral Branches. Mol Cell Neurosci 84, 36–47. https://doi.org/10.1016/j.mcn.2017.03.007.
8. Li, W., Lipsius, K., Burns, N.G., Sato, R., Rehman, A., Xue, H., Combs, C., Minichiello, L., Gangrade, H., Tampakakis, E., et al. (2024). Vascular smooth muscle cell-derived nerve growth factor regulates sympathetic collateral branching to innervate blood vessels in embryonic skin. Biol Open 13, bio060147. https://doi.org/10.1242/bio.060147.
9. Shafi, M.M., Vernet, M., Klooster, D., Chu, C.J., Boric, K., Barnard, M.E., Romatoski, K., Westover, M.B., Christodoulou, J.A., Gabrieli, J.D.E., et al. (2015). Physiological consequences of abnormal connectivity in a developmental epilepsy. Ann Neurol 77, 487–503. https://doi.org/10.1002/ana.24343.

10. Proietti Onori, M., Koene, L.M.C., Schäfer, C.B., Nellist, M., de Brito van Velze, M., Gao, Z., Elgersma, Y., and van Woerden, G.M. (2021). RHEB/mTOR hyperactivity causes cortical malformations and epileptic seizures through increased axonal connectivity. PLoS Biol 19, e3001279. https://doi.org/10.1371/journal.pbio.3001279.
11. Liu, J., Yang, X., Jiang, L., Wang, C., and Yang, M. (2012). Neural plasticity after spinal cord injury. Neural Regen Res 7, 386–391. https://doi.org/10.3969/j.issn.1673-5374.2012.05.010.
12. Yu, Y., Zhang, P., Han, N., Kou, Y., Yin, X., and Jiang, B. (2016). Collateral development and spinal motor reorganization after nerve injury and repair. Am J Transl Res 8, 2897–2911.
13. Chelyshev, Y.A., Kabdesh, I.M., and Mukhamedshina, Y.O. (2022). Extracellular Matrix in Neural Plasticity and Regeneration. Cell Mol Neurobiol 42, 647–664. https://doi.org/10.1007/s10571-020-00986-0.
14. Szebenyi, G., Callaway, J.L., Dent, E.W., and Kalil, K. (1998). Interstitial Branches Develop from Active Regions of the Axon Demarcated by the Primary Growth Cone during Pausing Behaviors. The Journal of Neuroscience 18, 7930–7940. https://doi.org/10.1523/jneurosci.18-19-07930.1998.
15. Flynn, K.C., Pak, C.W., Shaw, A.E., Bradke, F., and Bamburg, J.R. (2009). Growth cone-like waves transport actin and promote axonogenesis and neurite branching. Dev Neurobiol 69, 761–779. https://doi.org/10.1002/dneu.20734.
16. Gallo, G., and Letourneau, P.C. (1998). Localized Sources of Neurotrophins Initiate Axon Collateral Sprouting. The Journal of Neuroscience 18, 5403–5414. https://doi.org/10.1523/jneurosci.18-14-05403.1998.
17. Huang, E.J., and Reichardt, L.F. (2003). Trk Receptors: Roles in Neuronal Signal Transduction. Annual Review of Biochemistry 72, 609–642. https://doi.org/10.1146/annurev.biochem.72.121801.161629.
18. Zweifel, L.S., Kuruvilla, R., and Ginty, D.D. (2005). Functions and mechanisms of retrograde neurotrophin signalling. Nat Rev Neurosci 6, 615–625. https://doi.org/10.1038/nrn1727.
19. Ketschek, A., and Gallo, G. (2010). Nerve Growth Factor Induces Axonal Filopodia through Localized Microdomains of Phosphoinositide 3-Kinase Activity That Drive the Formation of Cytoskeletal Precursors to Filopodia. The Journal of Neuroscience 30, 12185–12197. https://doi.org/10.1523/jneurosci.1740-10.2010.

20. Harrington, A.W., and Ginty, D.D. (2013). Long-distance retrograde neurotrophic factor signalling in neurons. Nat Rev Neurosci 14, 177–187. https://doi.org/10.1038/nrn3253.
21. Doubleday, B., and Robinson, P.P. (1994). Nerve growth factor depletion reduces collateral sprouting of cutaneous mechanoreceptive and tooth-pulp axons in ferrets. The Journal of Physiology 481, 709–718. https://doi.org/10.1113/jphysiol.1994.sp020475.
22. Mearow, K.M. (1998). The effects of NGF and sensory nerve stimulation on collateral sprouting and gene expression in adult sensory neurons. Exp Neurol 151, 14–25. https://doi.org/10.1006/exnr.1998.6791.
23. Zheng, B., and Tuszynski, M.H. (2023). Regulation of axonal regeneration after mammalian spinal cord injury. Nat Rev Mol Cell Biol 24, 396–413. https://doi.org/10.1038/s41580-022-00562-y.
24. Ro, L.S., Chen, S.T., Tang, L.M., and Chang, H.S. (1996). Local application of anti-NGF blocks the collateral sprouting in rats following chronic constriction injury of the sciatic nerve. Neurosci Lett 218, 87–90. https://doi.org/10.1016/s0304-3940(96)13109-8.
25. Cohen-Cory, S., Kidane, A.H., Shirkey, N.J., and Marshak, S. (2010). Brain-derived neurotrophic factor and the development of structural neuronal connectivity. Developmental Neurobiology 70, 271–288. https://doi.org/10.1002/dneu.20774.
26. Azevedo, F.A.C., Carvalho, L.R.B., Grinberg, L.T., Farfel, J.M., Ferretti, R.E.L., Leite, R.E.P., Filho, W.J., Lent, R., and Herculano-Houzel, S. (2009). Equal numbers of neuronal and nonneuronal cells make the human brain an isometrically scaled-up primate brain. Journal of Comparative Neurology 513, 532–541. https://doi.org/10.1002/cne.21974.
27. Hatten, M.E. (1999). Central nervous system neuronal migration. Annu Rev Neurosci 22, 511–539. https://doi.org/10.1146/annurev.neuro.22.1.511.
28. Gibson, D.A., and Ma, L. (2011). Developmental regulation of axon branching in the vertebrate nervous system. Development 138, 183–195. https://doi.org/10.1242/dev.046441.
29. Gasperini, R.J., Pavez, M., Thompson, A.C., Mitchell, C.B., Hardy, H., Young, K.M., Chilton, J.K., and Foa, L. (2017). How does calcium interact with the cytoskeleton to regulate growth cone motility during axon pathfinding? Mol. Cell. Neurosci. 84, 29–35. https://doi.org/10.1016/j.mcn.2017.03.006.
30. Goldberg, D.J., and Burmeister, D.W. (1992). Microtubule-based filopodium-like protrusions form after axotomy. J. Neurosci. Off. J. Soc. Neurosci. 12, 4800–4807. https://doi.org/10.1523/JNEUROSCI.12-12-04800.1992.

31. Pagrut, S. (2023). The Capping Activity of Eps8 Regulates Axonal F-Actin Patch Dynamics and the Formation of Collateral Branch.